© 2002 American Chemical Society, J. Phys. Chem. B, Franzen jp025616k Supporting Info Page 1

JP025616K

SUPPLEMENTARY MATERIAL

RECEIVED
FEB 11 2002
JOURNAL OF PHYSICAL CHEMISTRY

Supplementary Material

The Supplementary Material contains discussion that connects the perimeter model proposed to earlier work. It also contains a comparison of the data analysis by three possible methods.

1. The method of moments
2. The derivative method
   A. Scaled derivative method
   B. Multiple Gaussian band fitting
3. The Rigid Shift-Gaussian method

I. Relationship of the VS-PM model to previous studies by Koboyashi et al.

Koboyashi and co-workers applied a modified four-orbital model to porphyrin π–π^* transitions and iron charge transfer transitions in ferric heme. [1,2] There is significant quenching of the orbital angular momentum in the excited state of the ferric heme. Koboyashi has interpreted this in terms of mixing of a $a_{1u},a_{2u} \rightarrow d_\pi$ charge transfer state. This mixing reduces the magnitude of the angular momentum in the Q state the by roughly a factor of two. The reduction of the orbital angular momentum in the B state is larger still, a factor of four when compared to MbCO. Here we consider how the vibronic coupling perimeter model developed here can be related to the LCAO approach taken by Koboyashi. The model is particularly applicable since we treat exactly the same charge transfer transitions ($a_{1u},a_{2u} \rightarrow d_\pi$) in deoxy case that Koboyashi treats for ferric heme. To our knowledge, the deoxy case has been discussed anywhere in Koboyashi's original studies, which were done mainly on ferric hemes. The most anomalous observation is that the sign of the MCD effect is reversed in the deoxy Soret band. This indicates that the angular momentum is larger in the ground state than in the excited state. Deoxy Mb has a S=2 ground state. The orbital angular momentum in the ground state is determined by the electron in the d_{xy},d_{x2y2} orbital and d_{xz} ,d_{yz} , which contribute L = 2 and L = 1 around the z axis, respectively. We make the following abbreviations:

$d_{z2} = \sigma$
$d_{yz} = \pi'$
$d_{xz} = \pi$
$d_{xy} = \delta'$
$d_{x2-y2} = \delta$

Following Koboyashi we can identify the following states:

Ground State $|+4\underline{-4}+4\underline{-4}\ \sigma\pi\pi'\delta\delta'\underline{\delta'}\rangle$
Singlet B $|+4\underline{-4}+4\underline{-5}\sigma\pi\pi'\delta\delta'\underline{\delta'}\rangle\ \Delta L_z = \pm 1$
Singlet Q $|+4\underline{-4}+4\underline{+5}\sigma\pi\pi'\delta\delta'\underline{\delta'}\rangle\ \Delta L_z = \pm 9$
Triplet B $|+4\underline{-4}+4\underline{-5}\sigma\pi\pi'\delta\delta'\underline{\delta'}\rangle\ \Delta L_z = \pm 1$
Triplet Q $|+4\underline{-4}+4\underline{+5}\sigma\pi\pi'\delta\delta'\underline{\delta'}\rangle\ \Delta L_z = \pm 9$
CT(III) $|+4\underline{-4}+4\sigma\pi\pi'\underline{\pi}'\delta\delta'\underline{\delta'}\rangle\ \Delta L_z = \pm 5$

© 2002 American Chemical Society, J. Phys. Chem. B, Franzen jp025616k Supporting Info Page 2

CT(III) $|+4\underline{-4}+4\sigma\pi\pi'\underline{\pi'}\delta\delta'\underline{\delta'}\rangle$ $\Delta L_z = \pm 3$
CT(I) $|+4\underline{-4}+4\sigma\pi\pi'\delta\underline{\delta}\delta'\underline{\delta'}\rangle$ $\Delta L_z = \pm 6$
CT(I) $|+4\underline{-4}+4\sigma\pi\pi'\underline{\pi'}\delta\underline{\delta}\delta'\underline{\delta'}\rangle$ $\Delta L_z = \pm 2$

The above model assumes that the lowest d-orbital is $d_{xy} = \delta'$ and that band I involves a transition from a_{1u},a_{2u} to that orbital. Eaton's polarized single crystal data and the Mossbauer spectroscopy analysis of Parak et al. indicate otherwise that the d_{xz} and d_{yz} orbitals are split and that one of these is the lowest orbital. The xz is the doubly occupied d-orbital and we have the following configurations:

Ground State $|+4\underline{-4}+4\underline{-4}\ \sigma\pi\delta\delta'\pi'\underline{\pi'}\rangle$
Singlet B $|+4\underline{-4}+4\underline{-5}\sigma\pi\delta\delta'\pi'\underline{\pi'}\rangle$ $\Delta L_z = \pm 1$
Singlet Q $|+4\underline{-4}+4\underline{+5}\sigma\pi\delta\delta'\pi'\underline{\pi'}\rangle$ $\Delta L_z = \pm 9$
Triplet B $|+4\underline{-4}+4\underline{-5}\sigma\pi\delta\delta'\pi'\underline{\pi'}\rangle$ $\Delta L_z = \pm 1$
Triplet Q $|+4\underline{-4}+4\underline{+5}\sigma\pi\delta\delta'\pi'\underline{\pi'}\rangle$ $\Delta L_z = \pm 9$
CT(III) $|+4\underline{-4}+4\sigma\pi\underline{\pi}\delta\delta'\pi'\underline{\pi'}\rangle$ $\Delta L_z = \pm 5$
CT(III) $|+4\underline{-4}+4\sigma\pi\underline{\pi}\delta\delta'\pi'\underline{\pi'}\rangle$ $\Delta L_z = \pm 3$
CT(I) $|+4\underline{-4}+4\underline{-4}\underline{-5}\sigma\pi\delta\delta'\pi'\rangle$ $\Delta L_z = \pm 6$
CT(I) $|+4\underline{-4}+4\underline{-4}\underline{+5}\sigma\pi\delta\delta'\pi'\rangle$ $\Delta L_z = \pm 4$

The π–π^* transitions are clearly recognizable as satisfying the conditions of the PM. The vibronically coupled based in analogy with the Koboyashi model for ferric heme is shown to be bands III and I. The model presented in the paper gives a vibronic mechanism that couples the states with angular momentum change $\Delta L_z = \pm 3$ with the allowed π–π^* transition ($\Delta L_z = \pm 1$). Note that the band III excited state configuration has the appropriate symmetry to mix with the singlet B or Q excited states, but not with the ground state.

II. Comparison of Methods

We follow the nomenclature of Piepho and Schatz in the presentation of formulae derived from the book "Group Theory in Spectroscopy with Applications to Magnetic Circular Dichroism". [3] The MCD signal is given as:

$$\frac{\Delta A}{E} = \gamma \mu_B B \left(A_1 \left(-\frac{\partial f(E)}{\partial E} \right) + \left(B_0 + \frac{C_0}{kT} \right) f(E) \right) \tag{1}$$

which is also Eqn. 4.5.14 of P&S. The A_1 parameter is

$$A_1 = \frac{1}{g_A} \sum_{\alpha\lambda} \left(\left(\langle J\lambda | L + 2S | J\lambda \rangle - \langle A\alpha | L + 2S | A\alpha \rangle \right) \left(\langle A\alpha | m_{-1} | J\lambda \rangle^2 - \langle A\alpha | m_{+1} | J\lambda \rangle^2 \right) \right) \tag{2}$$

where g_A is the electronic degeneracy of the ground state (Eqn. 4.5.16 of P&S). [3] The dipole strength, $\langle D_0 \rangle$ is defined by:

$$\frac{A(E)}{E} = \gamma D_0 f(E) \tag{3}$$

where f(E) is the line shape function. The energy E can be expressed in wavenumbers, which we represent as ν in the following. The expressions given above for A_1 and D_0, are valid for an oriented sample. Using group theoretic methods Piepho and Shatz have shown that the isotropic averages of $\langle A_1 \rangle$ and $\langle D_0 \rangle$ are related to the values in Eqns. 1-3 by $\langle A_1 \rangle / \langle D_0 \rangle = (1/2) A_1/D_0$. The details of the treatment are given in Chapter 17 of P&S. The specific case of D_4 symmetry is treated on page 373 of P&S. Since the experimentally measured values correspond to the isotropic average we calculate the z-component of the angular momentum according to $L_z = 2\langle A_1 \rangle / \langle D_0 \rangle$. This equation is used to convert the experimentally determined values of $\langle A_1 \rangle$ and $\langle D_0 \rangle$ to angular momentum in Table 6.

II.A. Method of Moments

The method of moments is regarded as the "more rigorous" of the two possible methods they consider. We consider the alternative rigid-shift Gaussian model below. However, P&S also add that "it is simple to apply but requires discrete bands." (page 124 P&S). [3] We consider the ramifications of this comment in detail. The recommended procedure in Piepho and Schatz is a numerical integration of ΔA/ν and then A/ν to obtain the $\langle D_0 \rangle$ and $\langle A_1 \rangle$ parameters, respectively. Using Beer's law A = εcl so these two expressions are also proportional if Δε/ν and ε/ν are calculated as shown below. The treatment discussed here follows Appendix A of P&S (pages 534-538). [3]

1. Determine ν_0 from setting first moment of absorption to zero.
2. Determine $\langle A_1 \rangle$ from

$$\int \frac{\Delta\varepsilon_m(\nu)}{\nu}(\nu - \nu_0)d\nu = \langle \Delta\varepsilon_m \rangle_1 = 152.5\langle A_1 \rangle \tag{4}$$

3. Determine B_0 from

$$\int \frac{\Delta\varepsilon_m(\nu)}{\nu} d\nu \, \langle \Delta\varepsilon_m \rangle_0 = 152.5 \, \langle B_0 \rangle \tag{5}$$

1. Obtain $\langle D_0 \rangle$ from

$$\int \frac{\varepsilon(\nu)}{\nu} d\nu = \langle \varepsilon \rangle_0 = 326.6 \, \langle D_0 \rangle \tag{6}$$

$\Delta\varepsilon_m$ is in units of M^{-1} cm^{-1} T^{-1}

II.A.1. Analysis of the MbCO MCD data using the method of moments

Piepho and Schatz warn against the use of the method of moments for spectra that contain overlapping bands. The problem of overlapping bands is evident in the Q band spectrum of SWMbCO. The first moment, calculated using the normalized formula

$$\nu_0 = \frac{\int \Delta\varepsilon_m(\nu)\nu d\nu}{\int \Delta\varepsilon_m(\nu) d\nu} \qquad (7)$$

is shown in Figure 1.

The slope of the plotted Eqn. 7 that is evident arises due to the fact that the bands are not individual bands. Thus, the integration does not begin or end with zero intensity. As a consequence there is uncertainty in the determination of ν_0. The uncertainty in ν_0 is ±5% in the Q band and ±2% in the Soret band. These uncertainties are quite significant since the interpretation of the integrated MCD signal will be vastly different for different values of ν_0. Due to the overlapping band problem the zero crossing of the MCD was used as the first moment ν_0. The estimates are 23719 cm^{-1} and 17507 cm^{-1} for the Soret and Q band, respectively.

A plot of $\varepsilon(\nu)/\nu$ is shown in Figure 2 and the integrated curves, $\int\varepsilon(\nu)/\nu\, d\nu$ as indicated in Eqn. 6 are given in Figure 3. Note that it is difficult to determine exactly where the integration for the Q band should end and that for the Soret band should begin. The lines shown are at 1800 and 12500, so the integrated values for Q and B bands are 1800 and 10700, respectively. The error in these values is estimated at 6% and 5% for the Q and B bands, respectively. $\langle D_0\rangle$ = 10700/326.6 for the Soret band and 1800/326.6 for the Q band. Using these estimates for $\int\varepsilon(\nu)/\nu d\nu = 326.6\langle D_0\rangle$, we obtain 5.5±0.3 D^2 and 32.8±1.6 D^2, respectively.

Determination of the A_1 parameter in MCD is based on determining the first moment of the MCD signature. The steps are shown in Figures 4-8 below. Figure 4 shows the MCD signal with wavenumber weighting, $\Delta\varepsilon(\nu)/\nu$. Figure 5 shows the first moment function for the Q band MCD signal, $\Delta\varepsilon(\nu)/\nu(\nu - \nu_0)$. The function shown in Figure 5 represents the integrand of the first moment expression (Eqn. 4). Figure 6 shows the integrated first moment.

Based on the weighted MCD data shown in Figure 4 the same procedure can be carried out for the B (Soret) band. The first moment function is shown in Figure 7. Figure 8 shows the integrated value of this function over the Soret band region.

Because of the vibronic structure in the Q band and the overlap of the Q band with the Soret, it is difficult to quantitatively interpret the data shown in Figures 5-8. The reason for this is that it is not clear where the vibronic progression of the Q band ends. There is clearly a great deal of intensity as much as 3000 cm^{-1} above ν_0. With this caveat, the values of obtained are $\langle A_1\rangle \approx 2000/152.5 = 13.1$ and $\langle A_1\rangle \approx 1800/152.5 = 11.8$ for the Q and Soret bands, respectively. The estimated uncertainty in these values is ±8% and ±12%, respectively. Including propagation of error, the ratio of $\langle A_1\rangle/\langle D_0\rangle$ is 2.38±0.22 and 0.36±0.05 for the Q and Soret bands, respectively. According to this analysis the relative magnitude of the angular momentum is approximately 6.6 times larger in the Q band than in the Soret band.

II.A.2. Analysis of the deoxy Mb MCD data using the method of moments

Application of the method of moments to deoxy Mb follows the same set of steps. The determination of ν_0 from the first moment of the absorption spectrum is, if anything, more difficult for deoxy Mb than for SWMbCO. The uncertainties in the band limits are shown in Figure 9. Figure 9 shows that the absorption bands of deoxy Mb are broader than those for SWMbCO and that they have a greater degree of overlap than SWMbCO. For the Q band we can establish that ν_0 ranges somewhere between 17500 cm^{-1} and 18500 cm^{-1}. For the Soret band there is a greater degree of uncertainty. The values range in the region 22500 - 24500 cm^{-1}. The errors are ±5% and ±4% for Q and Soret bands, respectively.

The analysis in terms of moments starts with a determination of the dipole strength for the deoxy Q and Soret bands. We first plot the ν-weighted extinction coefficient. The integrated absorption spectrum shown in Figure 11. Figure 11 shows the difficulty in determining the dipole strength, $\langle D_0 \rangle$ for the Q and B transitions pf deoxy heme. It is difficult to delineate the limit of the integral over the band. While this is a problem for the Q band and it is especially difficult for the Soret band. The reason for this is that the vibronic bands are much more important in deoxy heme than in the low spin heme of SWMbCO. Figure 11 gives values of approximately 2300±200 and 16700±2350, which correspond to dipole strengths $\langle D_0 \rangle$ of 7.04±0.6 and 51.1±7.1 for the Q and Soret bands, respectively.

The determination of the A_1 parameter for deoxy heme also has considerable uncertainty due to the vibronic structure of the deoxy Mb MCD signals. The procedure for scaling and integration of the MCD signal is shown in Figures 12-14 and Figures15-17 for the Q and B bands, respectively. The integrated values obtained from Figures 14 and 17 are 1300/152.5 = 8.52±1.2 and 5700/152.5 = -25.5±4.0, respectively. These values correspond to $\langle A_1 \rangle$ = 8.52 and $\langle A_1 \rangle$ = -25.5 for the Q and B bands, respectively. Comparing these values to the above values we obtain $\langle A_1 \rangle / \langle D_0 \rangle$ = 2.59±0.4 and $\langle A_1 \rangle / \langle D_0 \rangle$ = -1.06±0.22 for the Q and B bands, respectively.

II.B. Scaled Derivative Method

An alternative to the approach taken above is a model-free approach where the raw derivative of the absorption spectrum is used. This is justified using the nomenclature of Piepho and Schatz. If we divide the equation for the A_1 parameter (Eqn. 1) by the equation for the dipole strength (Eqn. 3) we obtain:

$$\frac{\frac{\Delta A}{E}}{\frac{A(E)}{E}} = \frac{\gamma \mu_B B\left(A_1\left(-\frac{\partial f(E)}{\partial E}\right)\right)}{\gamma D_0 f(E)}$$

or

$$\frac{\Delta A}{A(E)} = \frac{A_1 \mu_B B}{D_0} \frac{\left(-\frac{\partial f(E)}{\partial E}\right)}{f(E)}$$

Given that ΔA is reported in units of $M^{-1}cm^{-1}T^{-1}$ the magnetic field B can be eliminated. Applying this equation, we have a direct empirical determination of $\langle A_1 \rangle / \langle D_0 \rangle$ based on the numerical derivative of the lineshape function f(E). The procedure is to take the derivative of f(E) and then to find the scale factor for that derivative that best matches ΔA. The scale factor is equal to $\langle A_1 \rangle \mu_B / \langle D_0 \rangle$. μ_B is conveniently represented as 0.4669 $cm^{-1}T^{-1}$. Since ΔA is expressed in a per tesla basis the scale factor is $0.4669 \langle A_1 \rangle / \langle D_0 \rangle$.

II.B.1. Application to MbCO

Application of the scaled derivative method to the MCD signal of SWMbCO is shown in Figures 18 and 19 for the Q band Soret band, respectively. After taking the derivative of absorption spectrum The derivatives were multipled by -1.20±0.04 and -0.23±0.01 to correspond to the MCD data. These scaling factors correspond to $(\partial f(\nu)/\partial \nu)/ f(\nu)$. When scaled by the magnetic field, B as indicated above the values of $\langle A_1 \rangle / \langle D_0 \rangle$ obtained with this method are 2.57 and 0.50, for the Q and Soret bands, respectively. With the exception of the 0-1 vibronic band (β band) the correspondence is quite good as shown in Figures 18 and 19. Based on this approach the magnitude of $\langle A_1 \rangle / \langle D_0 \rangle$ is 5.14 times larger in the Q band than in the Soret band.

II.B.1. Application to deoxy Mb

The same approach can be applied to deoxy Mb. The first derivative of the absorption spectrum is taken and scaled. The scaled derivatives are shown in Figures 20 and 21 for the Q and B bands, respectively. The scale factors applied were -1.0±0.04 and 0.9±0.03 for the Q and Soret bands, respectively. Note that the sign of the B band MCD is anomalous as reflected by the fact that the scaling factor has a positive sign. Based on this approach the Q band MCD signal is roughly 1.11 times larger than that of the Soret band and opposite in sign.

II.C. Multiple Gaussian Scaled Derivative Method

The method of moment and the scaled derivative method outlined above do not permit separate consideration of the vibronic bands. The entire line shape of a band must be used for comparisons between the magnitude of the absorption intensity and the MCD signal. This leads to disagreement between the line shape in some cases. This is particularly noticeable in the Q band of deoxy heme. This band is strongly vibronic and has 0-0, 0-1, 0-2 and even higher vibronic satellite bands. The method of moments provides an average over all of the vibronic bands. The derivative method may be scaled appropriately for the 0-0 transition, however, the higher vibronic bands will not fit as well. An alternative to these two methods is presented here as a Gaussian line shape model. The procedure consists of a fit of the absorption spectrum to a number of Gaussian functions. In an ideal case, each of these Gaussian functions would represent a vibronic band. Then the derivative of each of the Gaussians is taken and scaled

separately to reflect the fact that there can be orbital angular moment quenching in vibronic bands. In the following, the fits of the Q and Soret bands to 3 or 4 Gaussians is presented. The scaling parameters are also included in the Tables below.

II.C.1. Analysis of MbCO data

The Q band region of MbCO was fit to a four Gaussian model. The first three Gaussians in Table 1 account for most of the intensity in the α and β vibronic bands. The fourth Gaussian is required to fit the shoulder in the region between the Q bands and Soret band. The MCD was fit to a model in which the derivatives of each of the Gaussian bands was multiplied by a factor. The factor is equal to $\langle A_1 \rangle / \langle D_0 \rangle$ as discussed above for the other models.

Table 1. Parameters for a Gaussian fit to the MbCO Soret absorption and MCD spectra.

A	ν	Δν	$-(\partial f/\partial \nu)/ f$
3.323±0.12 e +06	17250±5	172±3	1.701±0.06
1.940±0.12 e +06	17615±11	191±7	1.406±0.13
4.907±0.28 e +06	18455±43	345±22	0.980±0.13
2.182±0.022e +07	18620±16	1047±15	0.250±0.19

The SWMbCO Soret band was fit to four Gaussians given in Table 2. The fourth Gaussian listed in Table 2 is centered at 21500 cm-1. This Gaussian is required to account for absorption intensity that lies between the Q and Soret bands. The significance of the fitted parameter for the derivative is unclear (row 4 and column 4 of Table 2). If this parameter is omitted entirely from the fit or if the Soret band is fit to three Gaussians, the magnitude of the remaining parameters is nearly the same.

Table 2. Parameters for a Gaussian fit to the MbCO Q band absorption and MCD spectra.

A	ν	Δν	$-(\partial f/\partial \nu)/ f$
1.87±0.2 e +07	23634±2	197±6	0.206±0.01
9.52±0.09 e +07	23661±7	356±23	0.250±0.005
1.21±0.02 e +08	24230±1	1083±4	0.171±0.01
3.34±0.09 e +07	21500 (fixed)	2500 (fixed)	3.81±0.22

Since each Gaussian component can vary independently, the Gaussian model can give rise to a MCD signal that is dependent on the vibronic band. The fit to the Q band can be considered as individual vibronic contributions. The 0-0 band is sharp and requires two Gaussians centered at 17250 cm^{-1} and 17615 cm^{-1}. The 0-1 band is represented by that Gaussian centered at 18455 cm^{-1}. If we compare the 0-0 band of both Q and Soret bands the ratio of their magnitudes is 6-7. The origin of the uncertainty is that there are two Gaussians required to fit the 0-0 transition of the Q band absorption. The values compare well to the derivative method that uses the experimental absorption spectra.

II.C.2. Analysis of deoxy Mb data

The deoxy heme absorption bands are extremely broad. The difficulty in interpretation of the line shape is clear from examination by the method of moments. There is ambiguity in the determination of the first moment due to the fact that Q band has a vibronic progression that extends to the Soret band. The Soret band is extremely broad and has significant intensity that overlaps with N and higher transitions. The MCD signal of the Soret band is apparently well represented by a first derivative of the absorption spectrum (see Figure 21). However, there is a small feature on the low energy side of the MCD signal that does not correspond to the first derivative. To accurately obtain this feature the Soret band was fit to four Gaussians, whose parameters are given in Table 4. Note that the sign of the first derivative that corresponds to the 0-0 vibronic band is reversed relative to the two higher terms. This suggests an additional complexity to the C-term MCD signal. It provides further evidence that the excited state splitting may have a vibronic origin. However, the correspondence between vibronic satellite peaks in the Q band and those in the Soret band are difficult to see. Attempts to model the Q band using four Gaussians proved ambiguous. Such a fit resulted in more than one Gaussian near 18,000 cm^{-1}. The fit to three Gaussians shown below suggests a vibronic satellite at 812 cm^{-1} and 1789 cm^{-1} above the 0-0 transition at 17050 cm^{-1}. The Soret band indicates two satellite vibronic bands at 464 cm^{-1}, and 929 cm^{-1}. The identity of the band near 26000 cm^{-1} in the fit to the deoxy Mb Soret spectrum is not known. This band seems too high in energy to be a vibronic band. It is nearly absent from the MCD spectrum suggesting that it may be a separate electronic transition.

Table 3. Parameters for a Gaussian fit to the deoxy Soret absorption and MCD spectra.

A	ν	Δν	$-(\partial f/\partial \nu)/ f$
3.88±0.07 e +07	22815±3	316±1	0.528±0.02
2.67±0.07 e +07	23279±7	350±2	-0.699±0.04
9.99±0.05 e +07	23744±2	786±2	-0.191±0.005
2.47±0.01 e +08	26060±26	2444±12	0.005±0.001

Table 4. Parameters for a Gaussian fit to the deoxy Q band absorption and MCD spectra.

A	ν	Δν	$-(\partial f/\partial \nu)/ f$
1.08±0.09 e +06	17050±14	282±11	2.006±0.16
7.61±0.24 e +06	17862±10	533±11	1.036±0.06
3.60±0.01 e +07	18839±12	1694±12	0.178±0.09

II.D. Rigid-Shift Gaussian Method

The approximation applied by Piepho and Schatz called the rigid-shift approximation Gaussian model (RS-G) is discussed in this section. It equivalent to the derivative method applied above where the absorption line shape and first derivative are scaled to determine the B_0, C_0 and A_1 parameters, respectively. The procedure is carried out following conversion of measured ΔA to [θ]. The steps are outlined below.

I. $\Delta A = A_{lcp} - A_{rcp}$

II. $\Delta A = \Delta\varepsilon\, lc$; $\Delta\varepsilon = \varepsilon_{lcp} - \varepsilon_{rcp}$
III. $[\theta] = 3300\,\Delta\varepsilon$
IV. $[\theta] = 21.349(f_A A_{i\to j} + f_B B_{i\to j} + f_B C_{i\to j}/kT)$
V. Then apply the equation

$$\Delta[\theta] = 32.44\left(\frac{2\nu_0 + \Delta\nu}{\Delta\nu^2}\right)A_{i\to j}$$

where ν_0 and $\Delta\nu$ arise from a Gaussian fit to the absorption spectrum. In Practice, the procedure is given in the following for the SWMbCO Soret band.

1. Go to the peak and then to the trough of the MCD data and get the wavenumber values to obtain an estimate for $\Delta\nu$. Subtract one from the other. For the Soret band of SWMbCO we have $\Delta\nu = 24010 - 23450 = 560\ cm^{-1}$.

2. From the absorption spectrum we obtain $\nu_0 = 23655\ cm^{-1}$.

3. Obtain the value of $[\theta]$ at the peak and at the trough using the above conversion steps. $\Delta[\theta] = 207070 - (-223870) = 430940$ per Tesla or 43.09 per gauss

4. Solve Eqn. V. for $A_{i\to j}$.

$$A_{i\to j} = \frac{\Delta[\theta]}{32.44\left(\frac{2\nu_0 + \Delta\nu}{\Delta\nu^2}\right)} = \frac{43.0940}{32.44\left(\frac{2(23655) + 560}{(560)^2}\right)} = 8.7$$

5. Obtain $D_{i\to j}$, the dipole strength (square of the transition moment) from Eqn. 3 above. The value obtained above for the MbCO Soret band is ≈30. There predicted ratio of $\langle A_1\rangle/\langle D_0\rangle$ is 8.7/30 ≈ 0.29. Application of the rigid-shift Gaussian model to the multiple vibronic bands of the Q band region is not meaningful since a single Gaussian cannot represent the absorption band. This has been demonstrated above where four Gaussians were required to fit the Q band of MbCO.

III. Summary of Experimental Methods

The methods used to fit the Q band and Soret bands are compared in Table 5 below. One major difference between the methods is that the multiple Gaussian method permits separate consideration of vibronic bands. The method of moments (MM) and scaled first derivative (SFD) method must both necessarily include all vibronic bands. They therefore present a kind of average over all of the bands present in a vibronic progression. The multiple Gaussian first derivative method (MG-FD) gives larger values for the $\langle A_1\rangle/\langle D_0\rangle$ ratio due to the fact that a particular vibronic band will have different orbital angular momentum quenching. The converted values of L_z are given in Table 6. The factor of two that arises is due to orientation averaging in a point group of D_4 symmetry appropriate for metalloporphyrins.

Table 5. Comparison of the ratio $\langle A_1 \rangle / \langle D_0 \rangle$ for the various methods.

Species	MM	SFD	MG-SFD	RS-G
MbCO Q	2.38±0.22	2.57±0.08	3.64±0.12	NA
MbCO Soret	0.36±0.05	0.50±0.02	0.44±0.02	0.29
Deoxy Mb Q	2.59±0.40	2.14±0.08	4.29±0.32	NA
Deoxy Mb Soret	-1.06±0.22	-1.92±0.06	-1.49±0.08	NA

Table 6. Comparison of the ratio L_z for the various methods.

Species	MM	SFD	MG-FD	RD-G
MbCO Q	4.76±0.44	5.14±0.16	7.28±0.24	NA
MbCO Soret	0.72±0.10	1.00±0.04	0.88±0.04	0.58
Deoxy Mb Q	5.18±0.80	4.28±0.16	6.58±0.64	NA
Deoxy Mb Soret	-2.12±0.44	-3.84±0.12	-2.98±0.16	NA

IV. Vibronic Coupling in the Free Electron Model

IV.A. Jahn-Teller Intrastate Coupling

The general case of mixing of degenerate PM states is given by a matrix element:

$$V = \left\langle \Phi_n \left| \frac{\partial V}{\partial R} \right| \Phi_{-n} \right\rangle \Delta R = \frac{1}{2\pi} \left\langle e^{in\phi} \left| \cos(2n\phi) \right| e^{-in\phi} \right\rangle k\Delta R^2 = \frac{k\Delta R^2}{2} \qquad \text{(A1)}$$

The energy of states 1 and –1 are equal. They are both given by:

$$H_{-n} = H_n = \left\langle \Phi_n \left| -\frac{\hbar^2}{2\mu R_0^2} \frac{\partial^2}{\partial \phi^2} \right| \Phi_n \right\rangle = \frac{\hbar^2 n^2}{2\mu R_0^2} \qquad \text{(A2)}$$

The eigenvalue problem for two degenerate states is given by:

$$\begin{pmatrix} H-\lambda & V \\ V & H-\lambda \end{pmatrix} = (H-\lambda)(H-\lambda) - V^2$$

$$\lambda^2 - (H+H)\lambda + H^2 - V^2 = 0$$

$$\lambda = \frac{2H \pm \sqrt{4H^2 - 4H^2 + 4V^2}}{2} \qquad \text{(A3)}$$

$$\lambda_+ = H + V$$

$$\lambda_- = H - V$$

The coefficients for the eigenvectors can be determined by substitution of the two eigenvalues into the matrix equation:

$-Vc_1 + Vc_2 = 0$

$c_1 = c_2$

$Vc_3 + Vc_4 = 0$

$c_3 = -c_4$

Normalization requires:

$c_1^2 + c_2^2 = 1$

$c_1 = 1/\sqrt{2}, c_2 = -1/\sqrt{2}$

$c_3^2 + c_4^2 = 1$

$c_3 = 1/\sqrt{2}, c_4 = 1/\sqrt{2}$ (A4)

The wave functions determined by degenerate perturbation theory are:

$$|E_x\rangle = \frac{1}{2\sqrt{\pi}}\left(\Phi_n + \Phi_{-n}\right) = \frac{1}{\sqrt{\pi}}\cos\left(n\phi\right)$$

$$|E_y\rangle = \frac{1}{2\sqrt{\pi}}\left(\Phi_n - \Phi_{-n}\right) = \frac{i}{\sqrt{\pi}}\sin\left(n\phi\right) \quad \text{(A5)}$$

IV.B. Herzberg-Teller Interstate Coupling

The general case of mixing of degenerate PM states is given by a matrix element:

$$V_{nn'} = \left\langle \Phi_n \left| \frac{\partial V}{\partial R} \right| \Phi_{-n'} \right\rangle \Delta R = \frac{1}{2\pi}\left\langle e^{in\phi} \left| \cos\left((n+n')\phi\right) \right| e^{-in'\phi} \right\rangle k\Delta R^2 = \frac{k\Delta R^2}{2} \quad \text{(B1)}$$

The energy of states 1 and –1 are equal. They are both given by:

$$H_n = \left\langle \Phi_n \right| -\frac{\hbar^2}{2\mu R_0^2}\frac{\partial^2}{\partial\phi^2} \left| \Phi_n \right\rangle = \frac{\hbar^2 n^2}{2\mu R_0^2}$$

$$H_{n'} = \left\langle \Phi_{n'} \right| -\frac{\hbar^2}{2\mu R_0^2}\frac{\partial^2}{\partial\phi^2} \left| \Phi_{n'} \right\rangle = \frac{\hbar^2 n'^2}{2\mu R_0^2} \quad \text{(B2)}$$

The eigenvalue problem for two degenerate states is given by:

$$\begin{pmatrix} H_n - \lambda & V \\ V & H_{n'} - \lambda \end{pmatrix} = \left(H_n - \lambda\right)\left(H_{n'} - \lambda\right) - V^2$$

$$\lambda^2 - \left(H_n + H_{n'}\right)\lambda + H_n H_{n'} - V^2 = 0$$

$$\lambda = \frac{\left(H_n + H_{n'}\right) \pm \sqrt{\left(H_n + H_{n'}\right)^2 - 4H_n H_{n'}^2 + 4V^2}}{2}$$

$$\lambda = \frac{\left(H_n + H_{n'}\right) \pm \sqrt{\left(H_n - H_{n'}\right)^2 + 4V^2}}{2} \quad \text{(B3)}$$

$\lambda_+ \approx H_n + V$

$\lambda_- \approx H_{n'} - V$

This same result can be obtained by perturbation theory. The wave functions for H-T VC are given by:

$$|E_n\rangle \approx \Phi_n + \frac{V}{H_n - H_{n'}}\Phi_{n'}$$

$$|E_{n'}\rangle \approx \Phi_{n'} - \frac{V}{H_n - H_{n'}}\Phi_n \quad \text{(B4)}$$

Application of the same procedure to the degenerate partners –n and –n' reverses the sign of the perturbation.

$$V_{-n,-n'} = \left\langle \Phi_{-n} \left| \frac{\partial V}{\partial R} \right| \Phi_{n'} \right\rangle \Delta R = \frac{1}{2\pi}\left\langle e^{i-n\phi} \left| \cos\left((n+n')\phi\right) \right| e^{in'\phi} \right\rangle k\Delta R^2 = -\frac{k\Delta R^2}{2} \quad \text{(B5)}$$

This results in opposite signs for the energy shift in the vibronically coupled excited states.

$$\lambda_+ \approx H_{-n} - V \qquad \text{(B6)}$$
$$\lambda_- \approx H_{-n'} + V$$

The coefficients of the perturbation theory wave functions are also reversed in sign.

$$|E_{-n}\rangle \approx \Phi_{-n} - \frac{V}{H_{-n} - H_{n'}}\Phi_{-n'} \qquad \text{(B7)}$$
$$|E_{-n'}\rangle \approx \Phi_{-n'} + \frac{V}{H_{-n} - H_{-n'}}\Phi_{-n}$$

References

(1) Koboyashi, H.; Shimizu, M.; Fujita, I. *Bull. Chem. Soc. Jpn.* **1970**, *43*, 2335-2341.
(2) Koboyashi, H.; Higuchi, T.; Eguchi, K. *Bull. Chem. Soc. Jpn.* **1976**, *49*, 457-463.
(3) Piepho, S. B.; Schatz, P. N. *Group Theory in Spectroscopy with Application to Magnetic Circular Dichroism*; John Wiley & Sons: New York, 1983.

© 2002 American Chemical Society, J. Phys. Chem. B, Franzen jp025616k Supporting Info Page 13

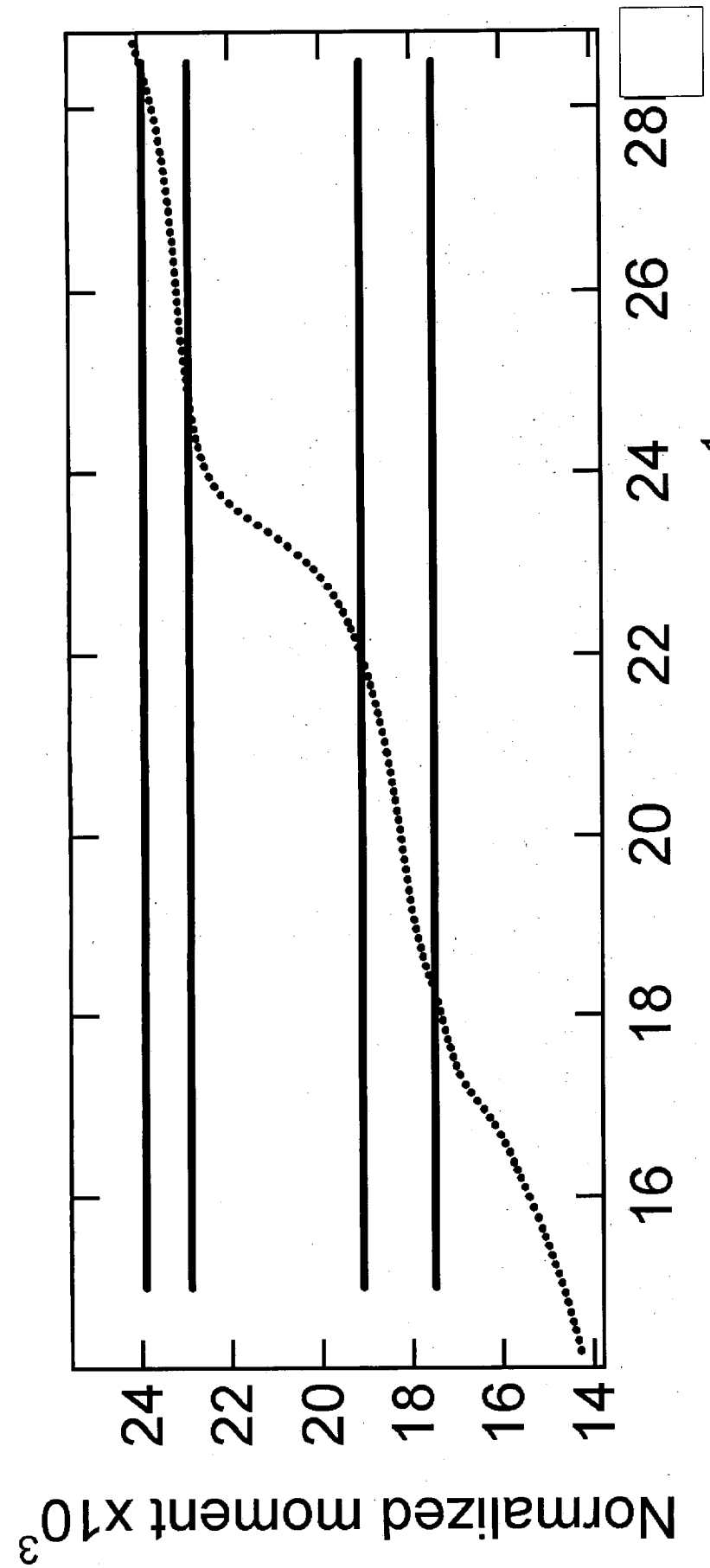

Figure 1. The normalized first moment of the SWMbCO absorption bands is plotted as a function of wavenumber. The solid lines represent the region from which ν_0 can be obtained.

© 2002 American Chemical Society, J. Phys. Chem. B, Franzen jp025616k Supporting Info Page 14

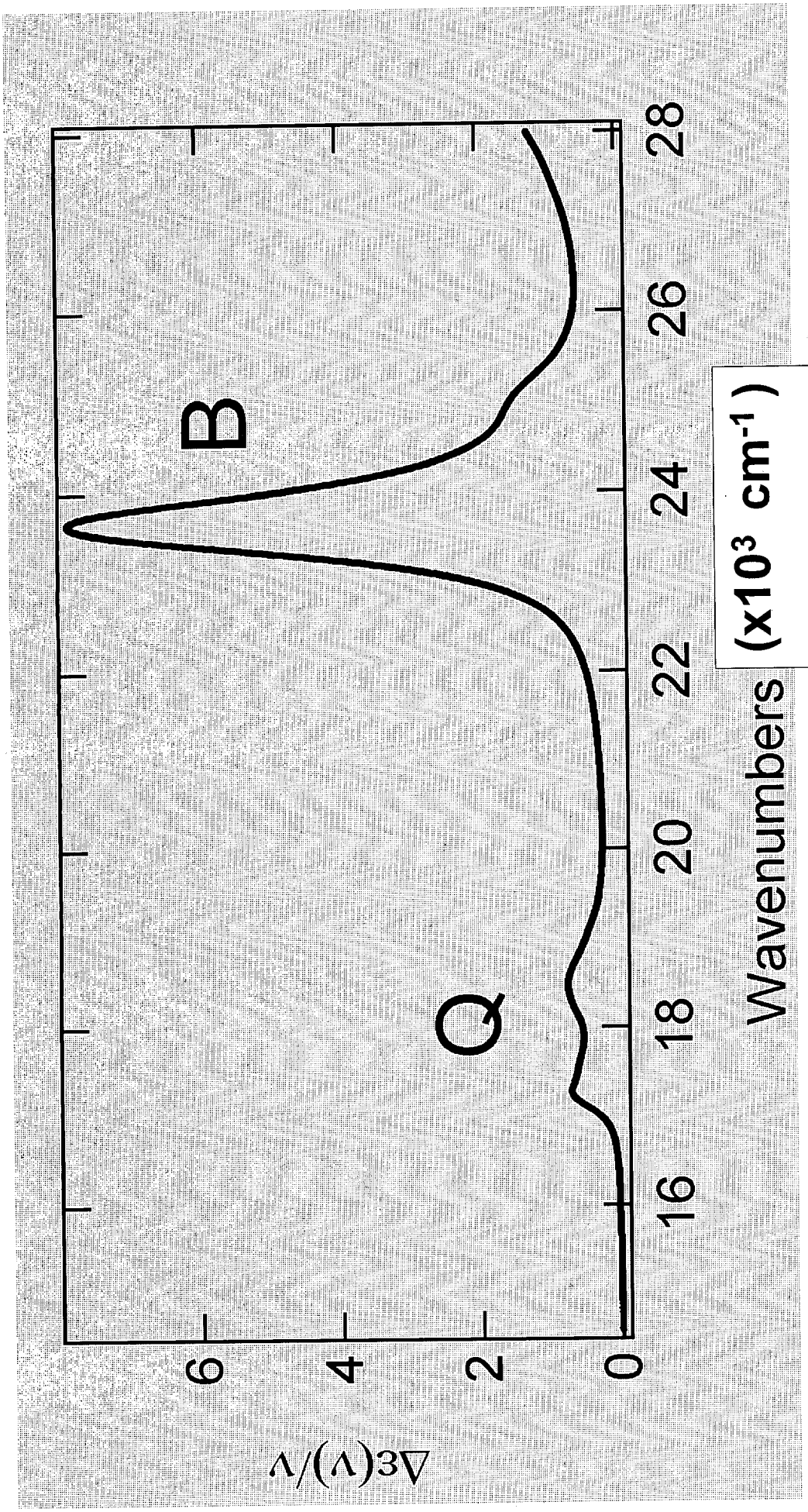

Figure 2. The energy-weighted extinction for MbCO is plotted as a function of wavenumber.

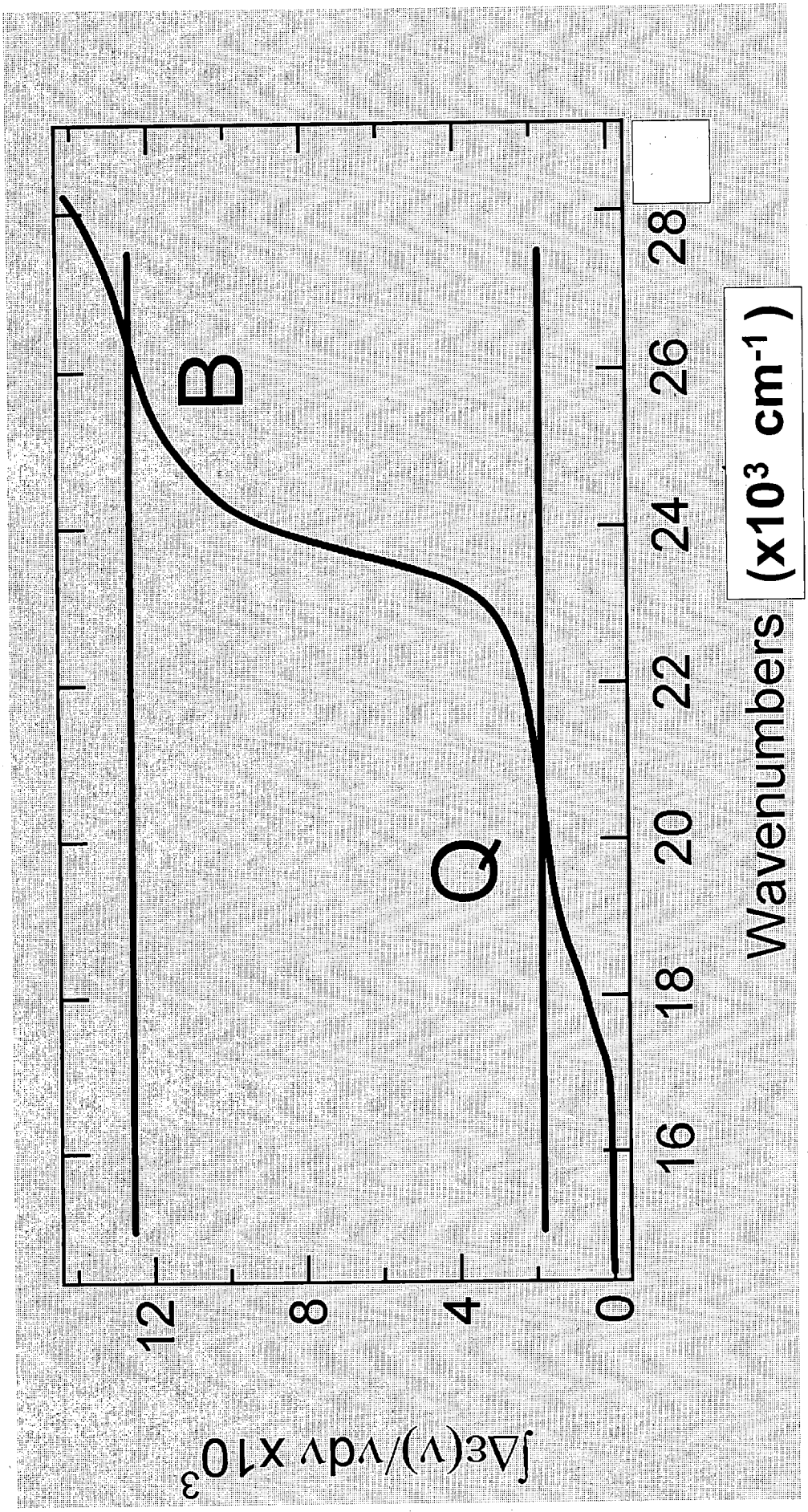

Figure 3. Integrated energy-weighted extinction curves are used to determine the dipole strength, D_0.

© 2002 American Chemical Society, J. Phys. Chem. B, Franzen jp025616k Supporting Info Page 16

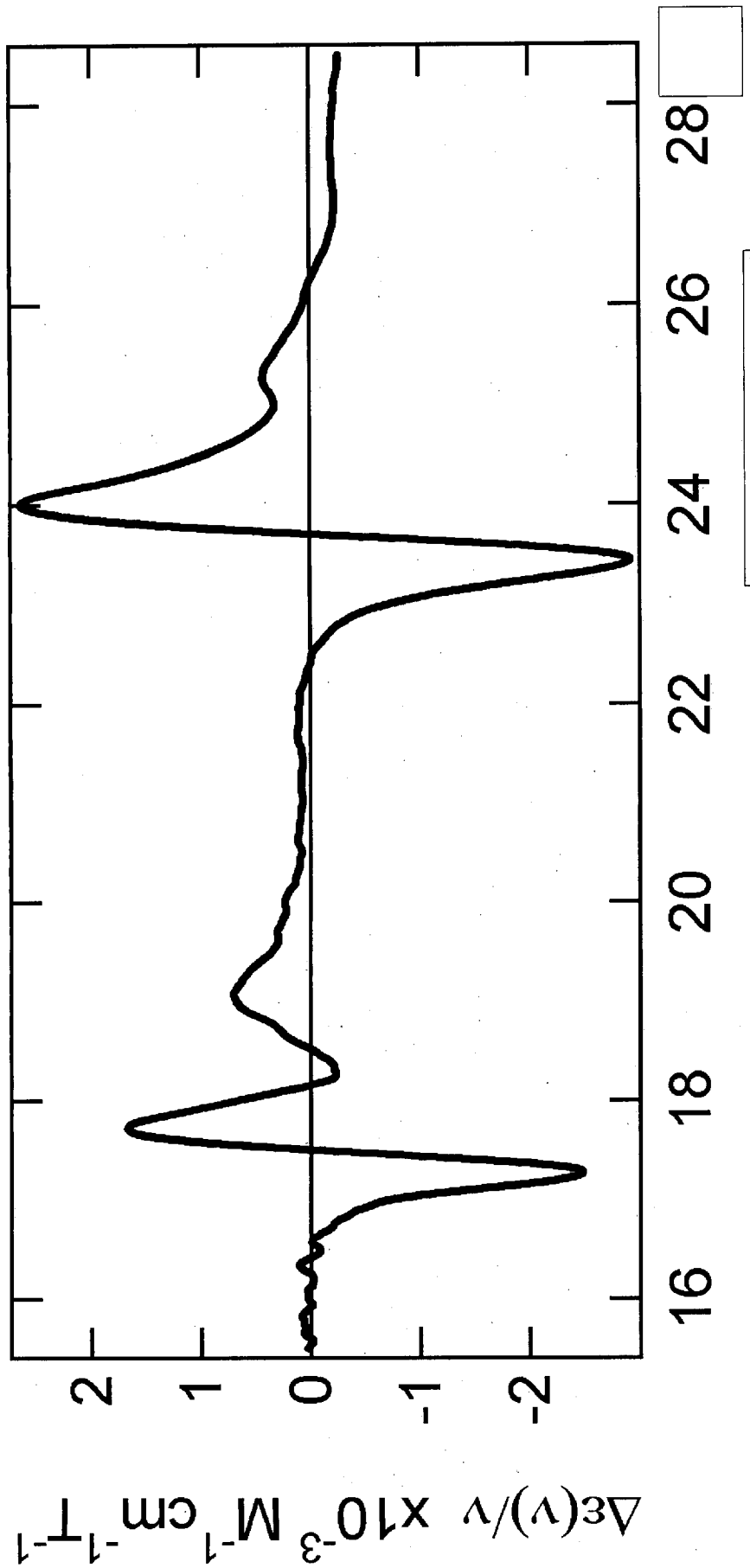

Figure 4. The energy-weighted MCD signal for MbCO is plotted.

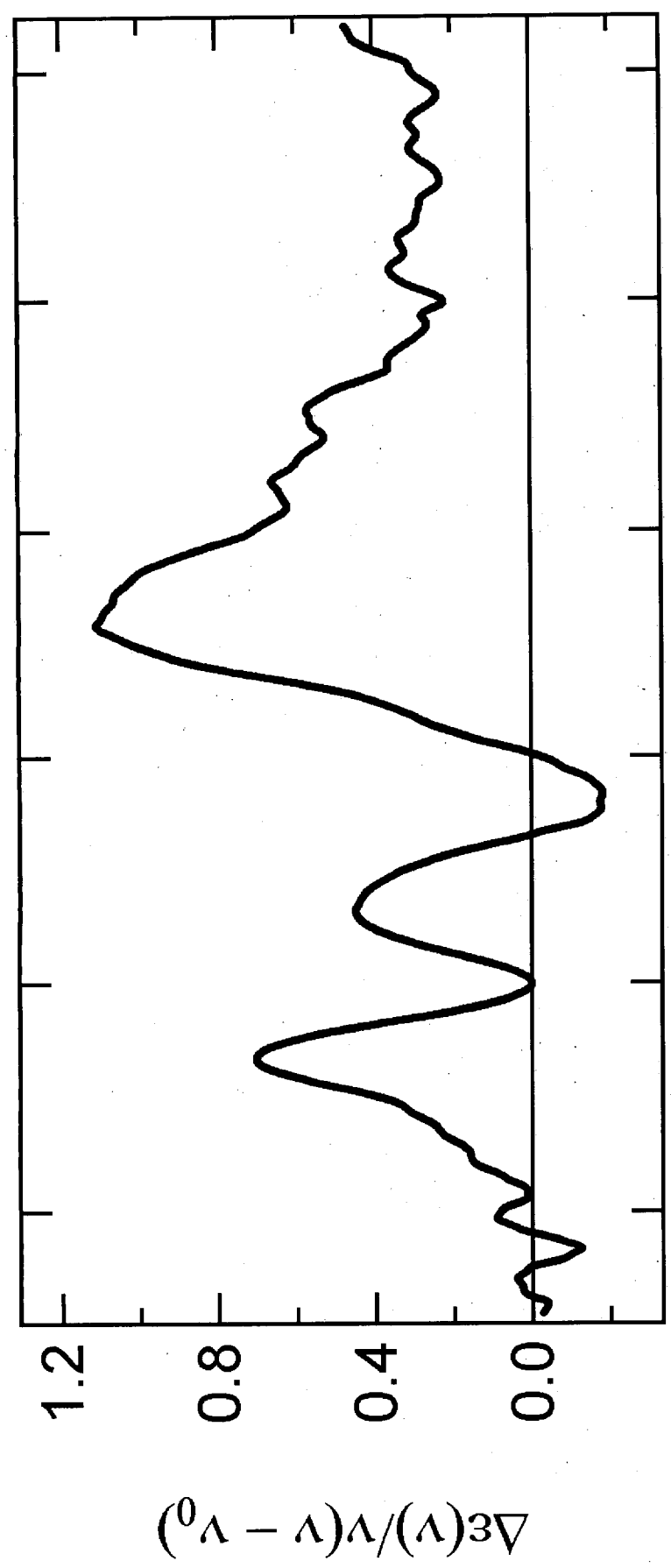

Figure 5. The integrand of the first moment of the MCD signal for the Q band of MbCO is plotted.

© 2002 American Chemical Society, J. Phys. Chem. B, Franzen jp025616k Supporting Info Page 18

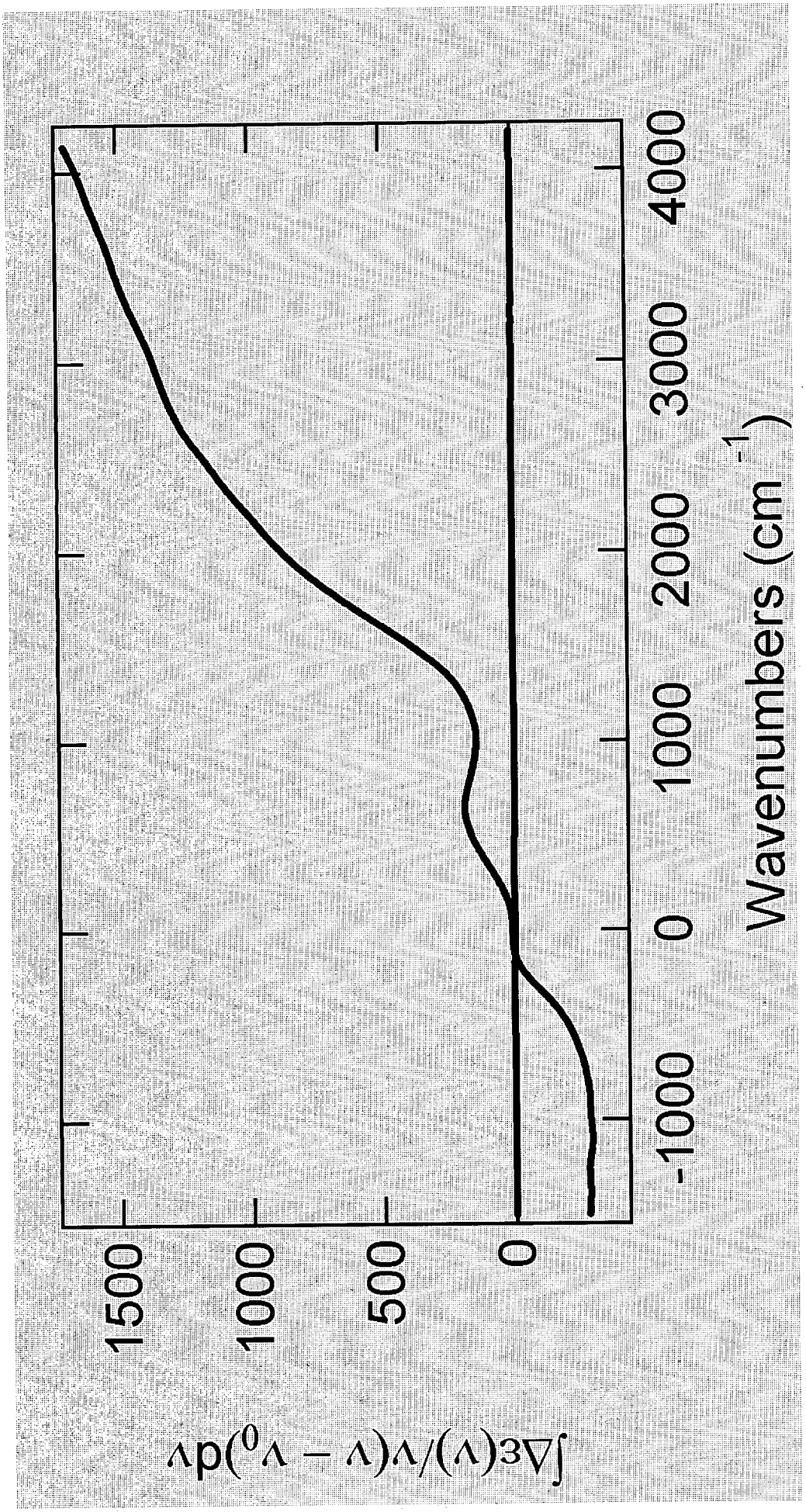

Figure 6. The integrated first moment of the MCD signal for the Q band of MbCO is plotted.

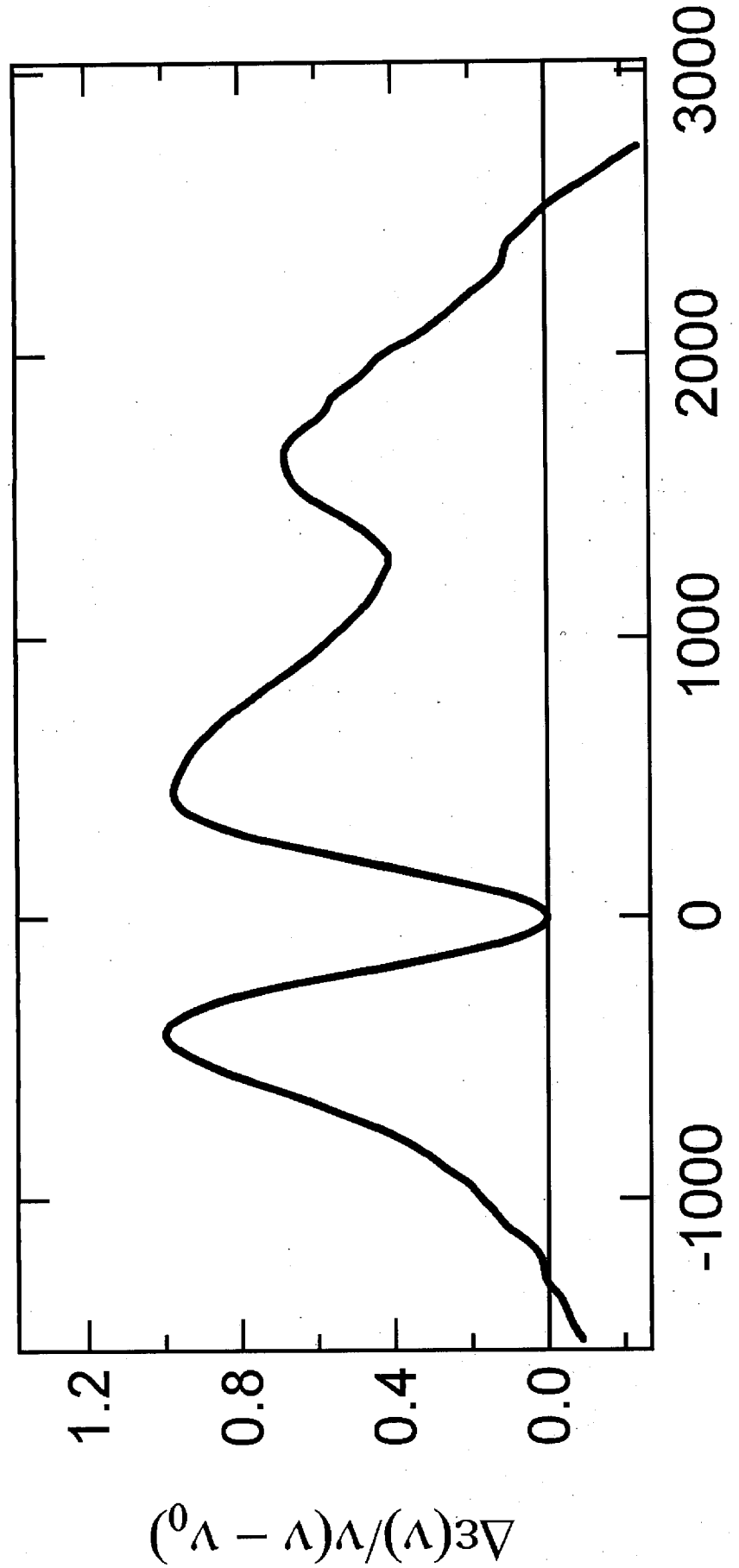

Figure 7. The integrand of the first moment of the MCD signal for the B band of MbCO is plotted.

© 2002 American Chemical Society, J. Phys. Chem. B, Franzen jp025616k Supporting Info Page 20

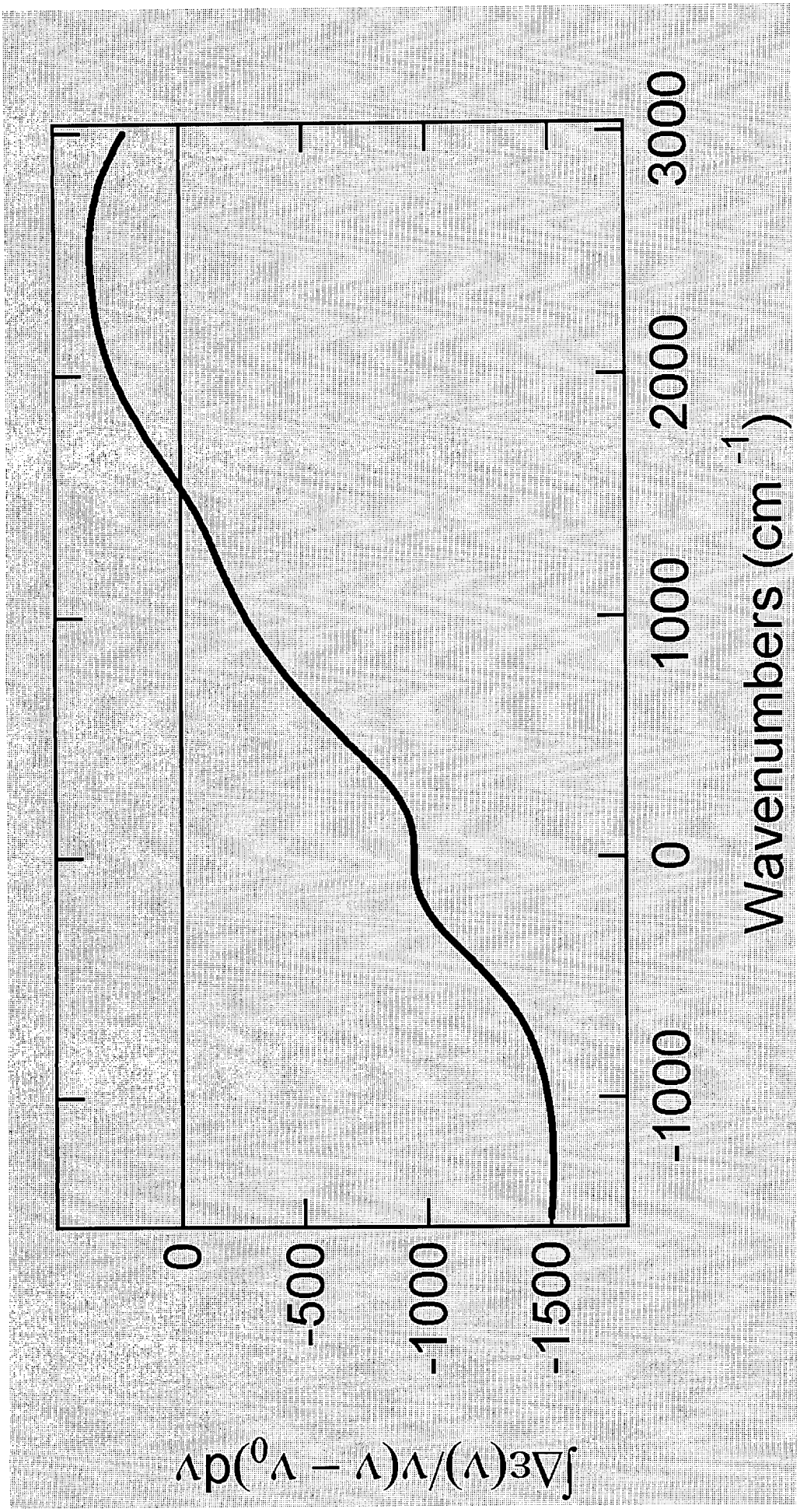

Figure 8. The integrated first moment of the MCD signal for the B band of MbCO is plotted.

© 2002 American Chemical Society, J. Phys. Chem. B, Franzen jp025616k Supporting Info Page 21

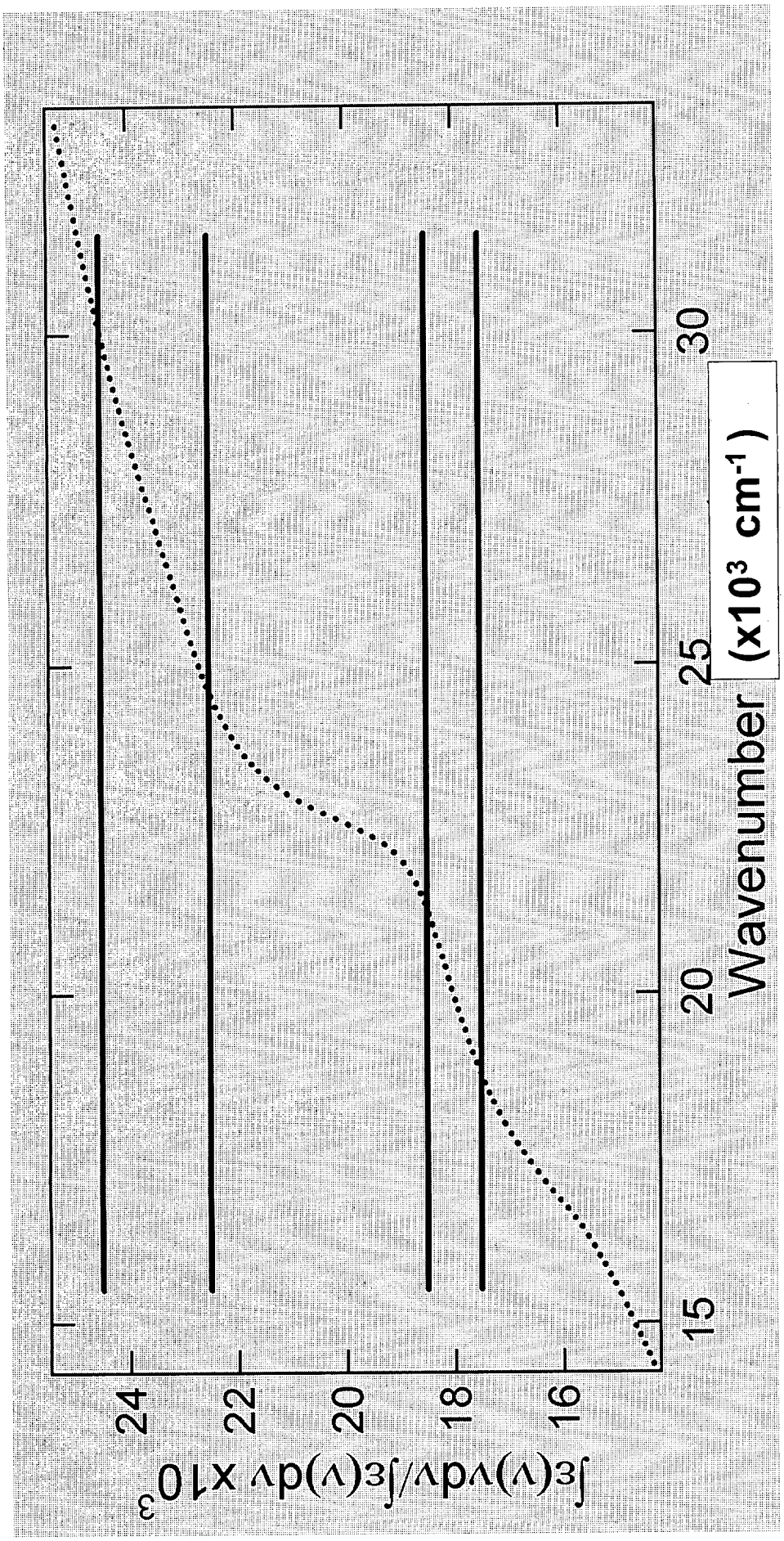

Figure 9. The integrated normalized first moment of the deoxy Mb absorption spectrum. The uncertainty in ν_0 is shown by the lines represented the high energy side of the Q and B bands.

© 2002 American Chemical Society, J. Phys. Chem. B, Franzen jp025616k Supporting Info Page 22

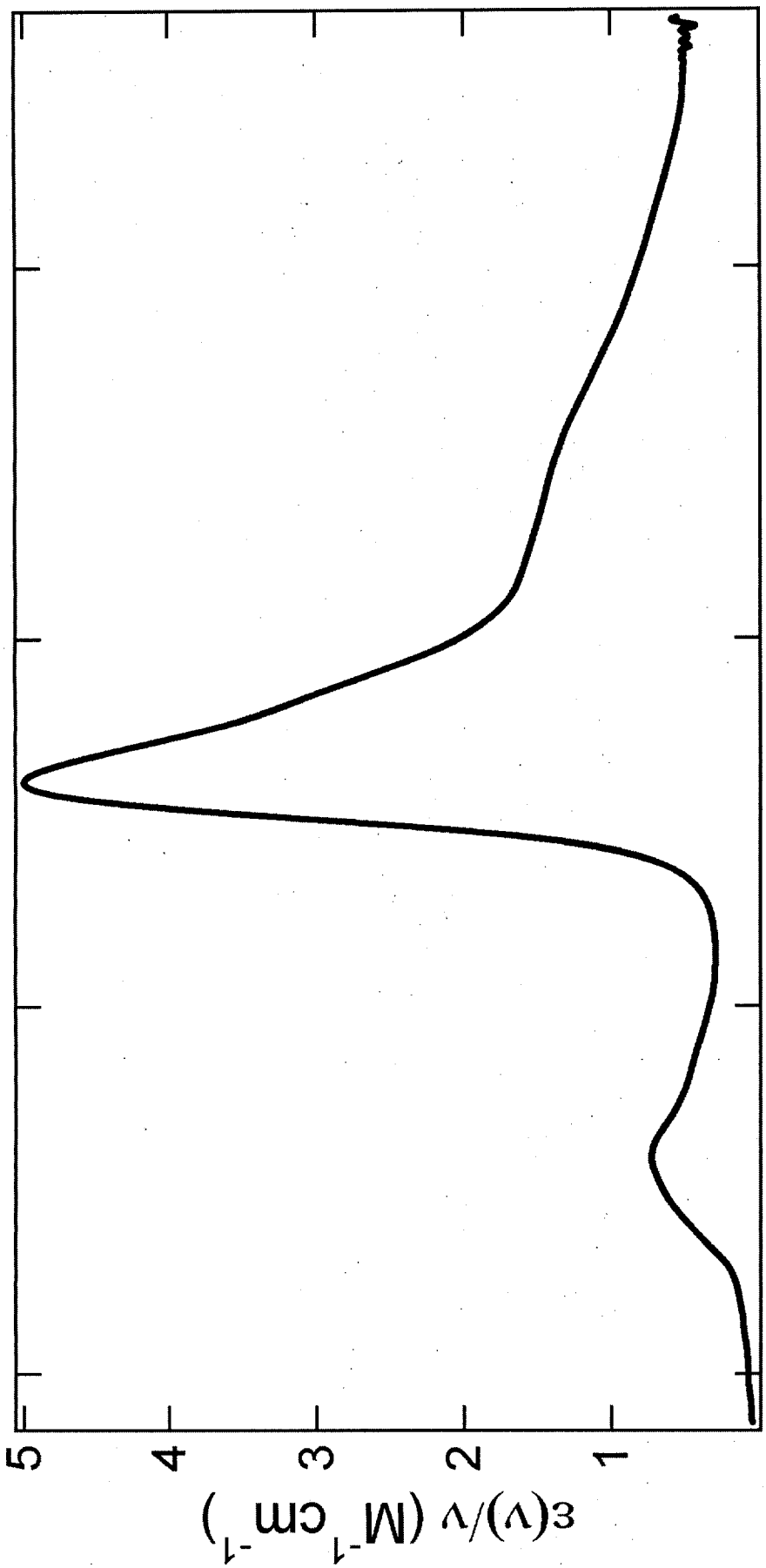

Figure 10. The energy-weighted absorption spectrum for deoxy Mb.

© 2002 American Chemical Society, J. Phys. Chem. B, Franzen jp025616k Supporting Info Page 23

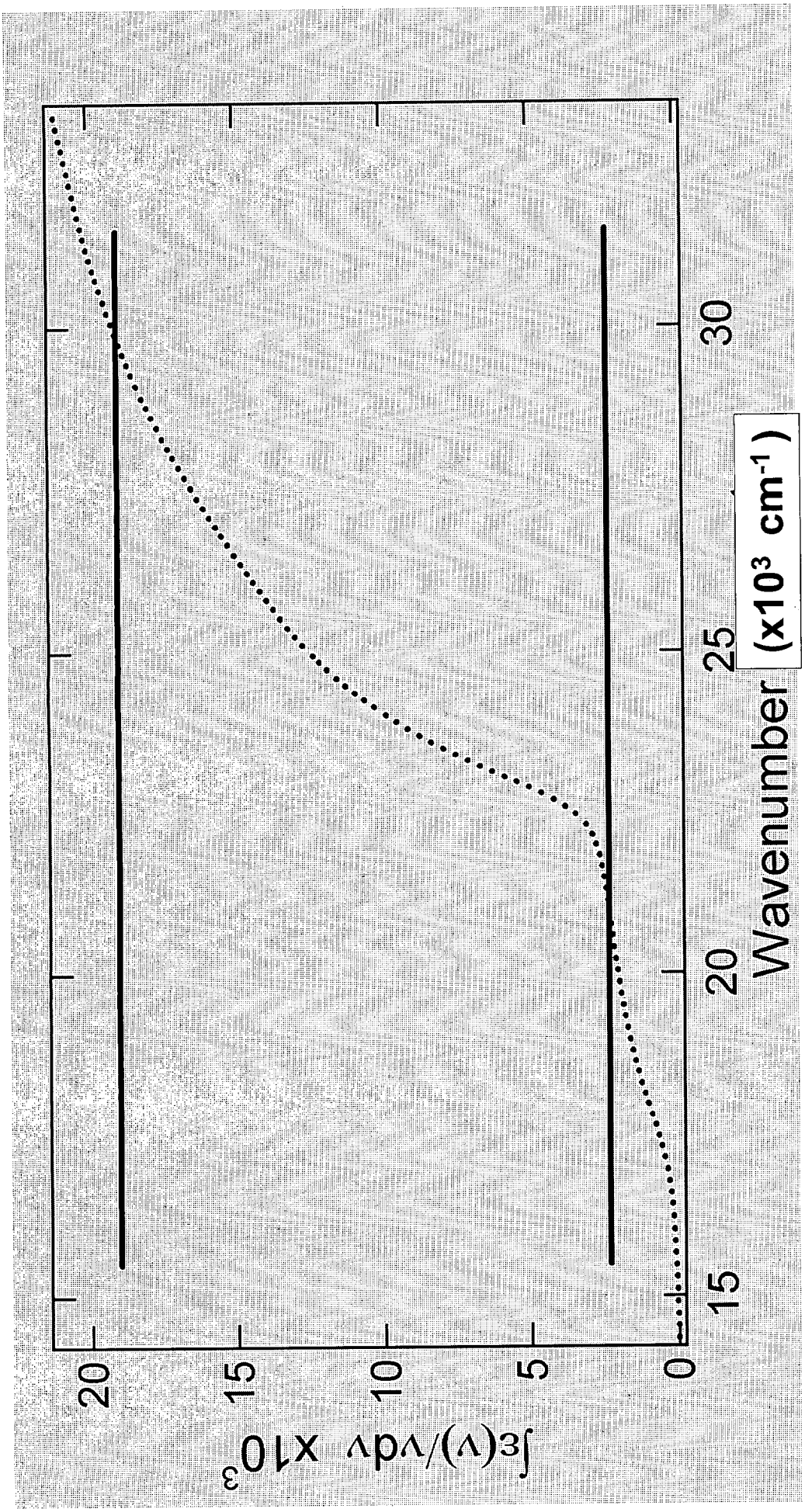

Figure 11. Integrated energy-weighted extinction curves are used to determine the dipole strength, D_0.

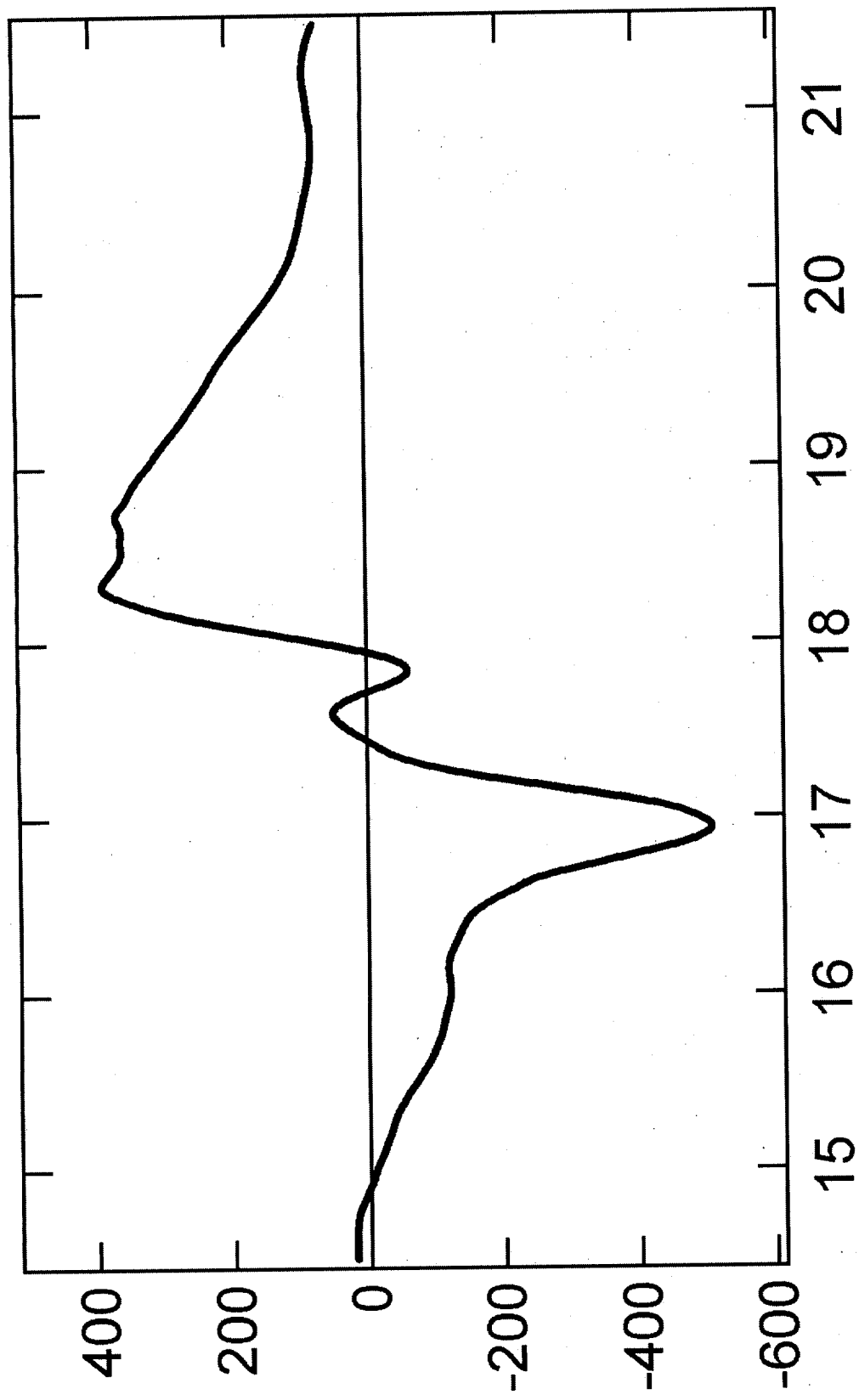

Figure 12. The energy-weighted MCD signal for the Q band of deoxy Mb is plotted.

© 2002 American Chemical Society, J. Phys. Chem. B, Franzen jp025616k Supporting Info Page 25

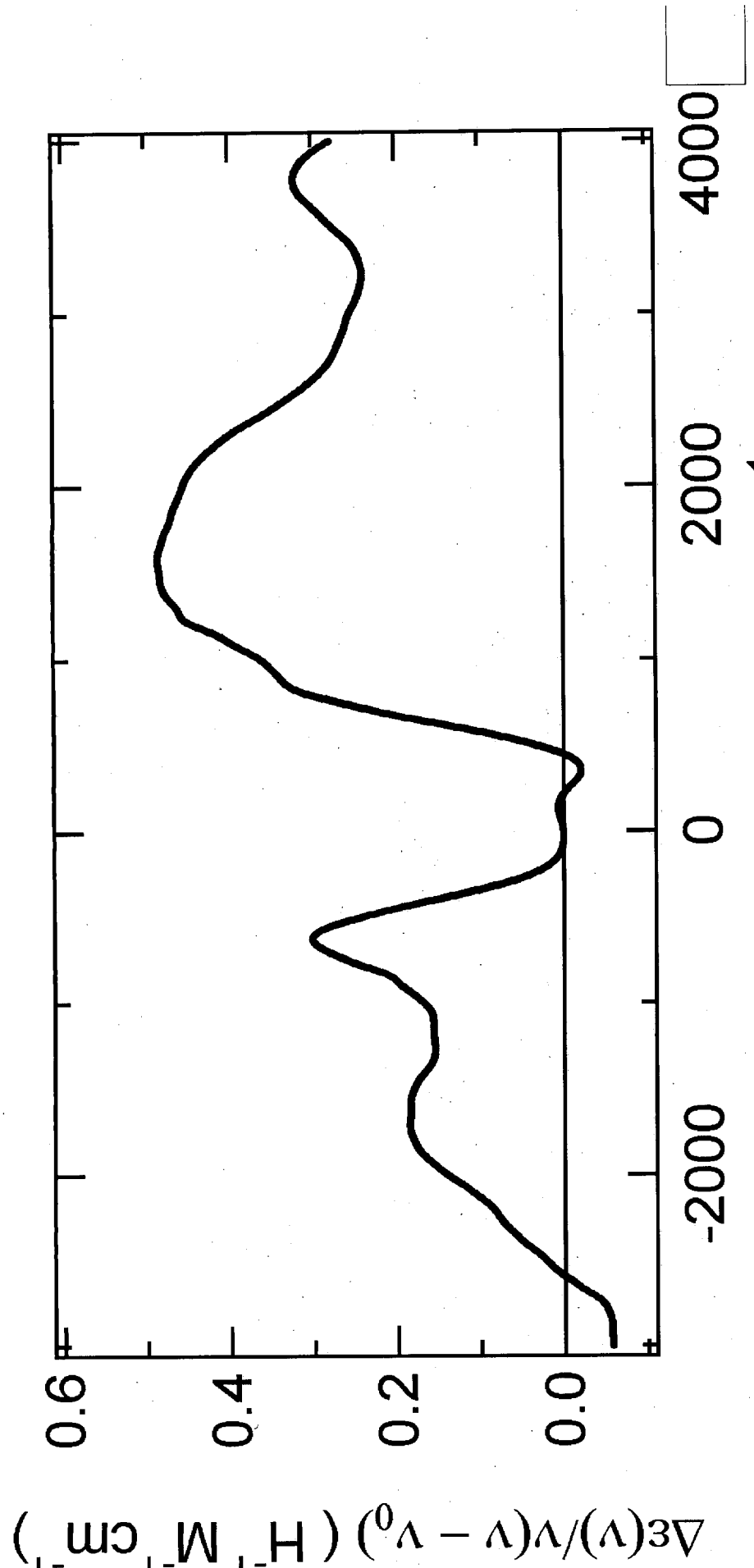

Figure 13. The integrand of the first moment of the MCD signal for the Q band of deoxy Mb is plotted.

© 2002 American Chemical Society, J. Phys. Chem. B, Franzen jp025616k Supporting Info Page 26

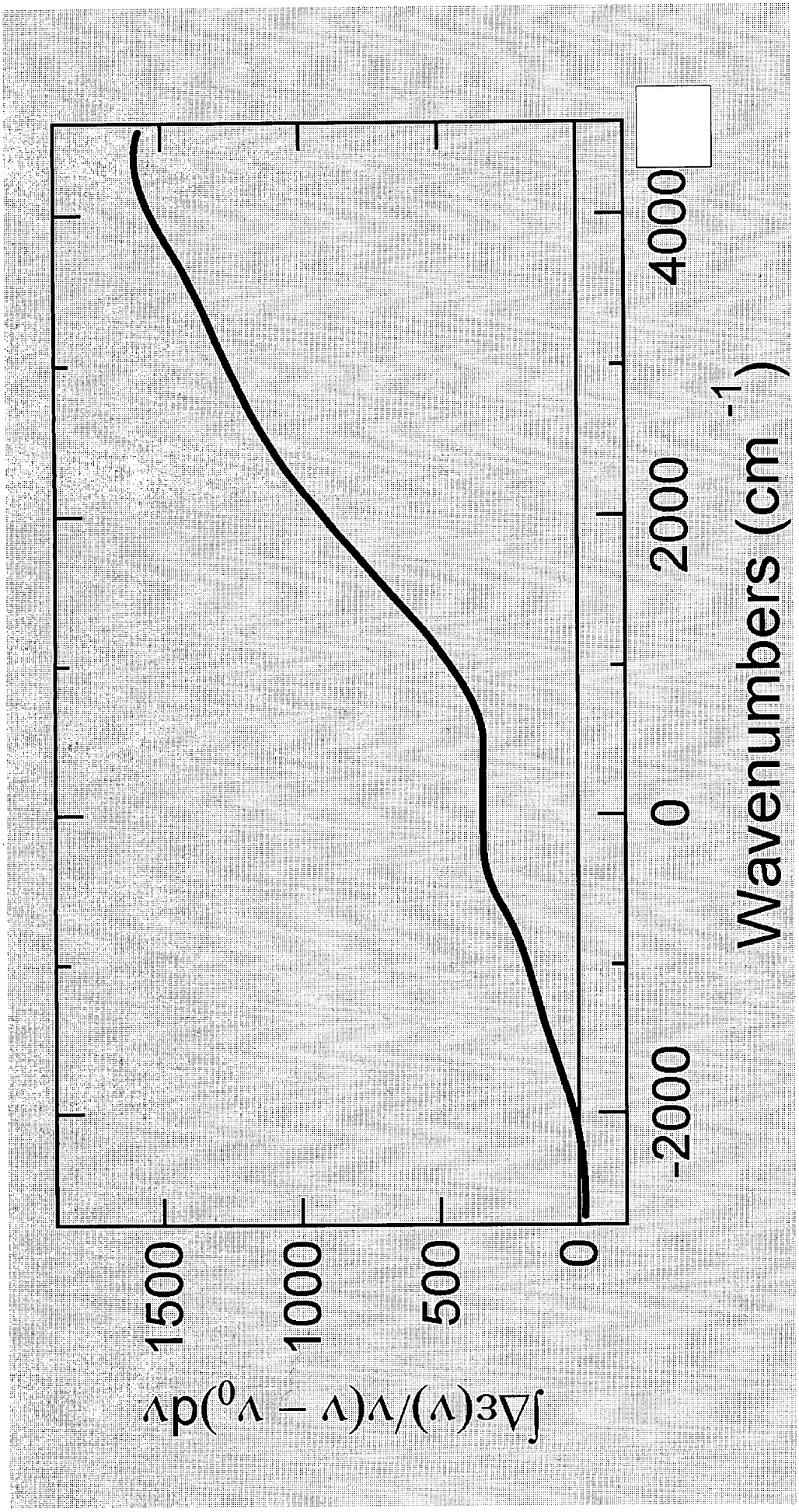

Figure 14. The integrated first moment of the MCD signal for the Q band of deoxy Mb is plotted.

© 2002 American Chemical Society, J. Phys. Chem. B, Franzen jp025616k Supporting Info Page 27

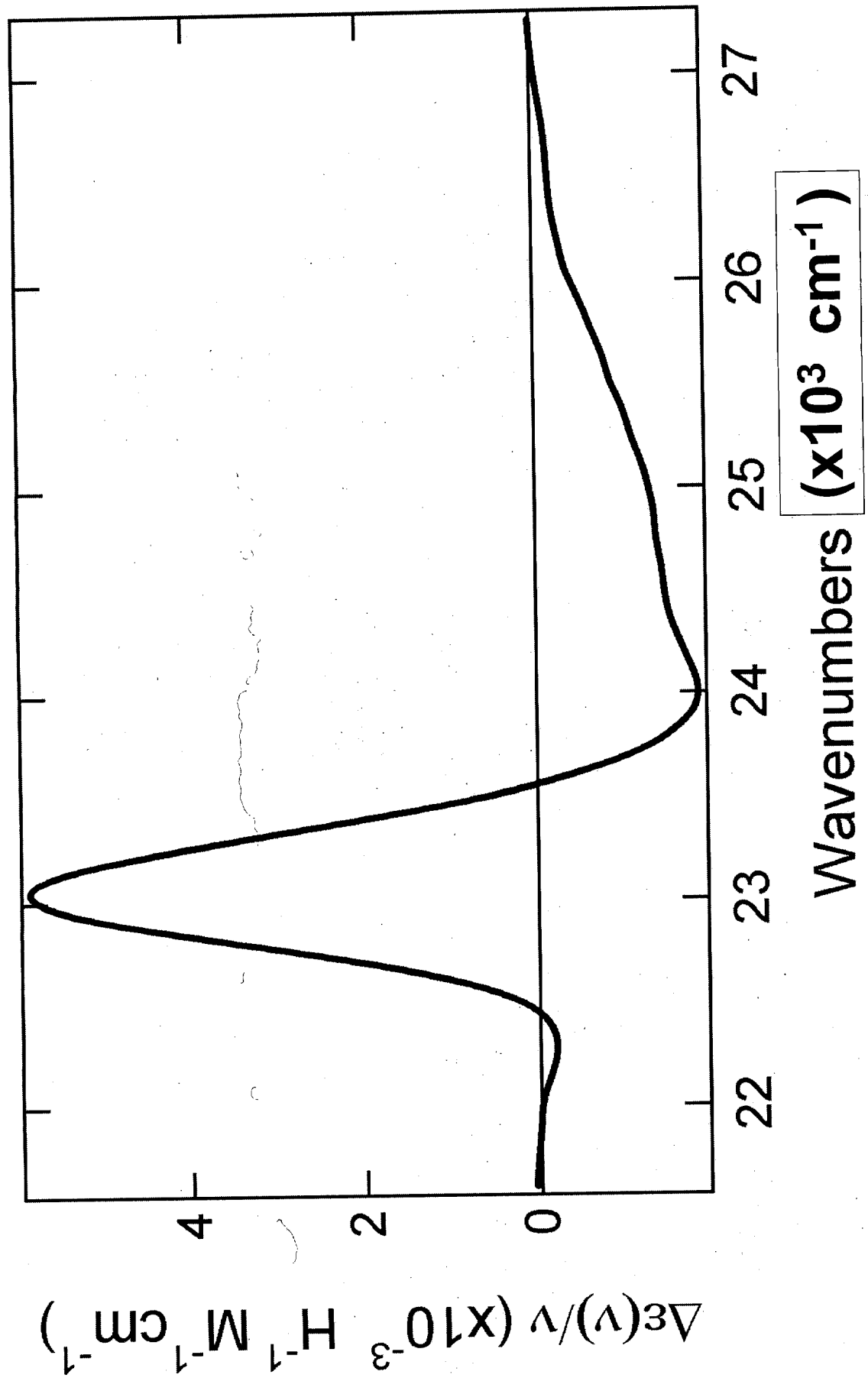

Figure 15. The energy-weighted MCD signal for the B band of deoxy Mb is plotted.

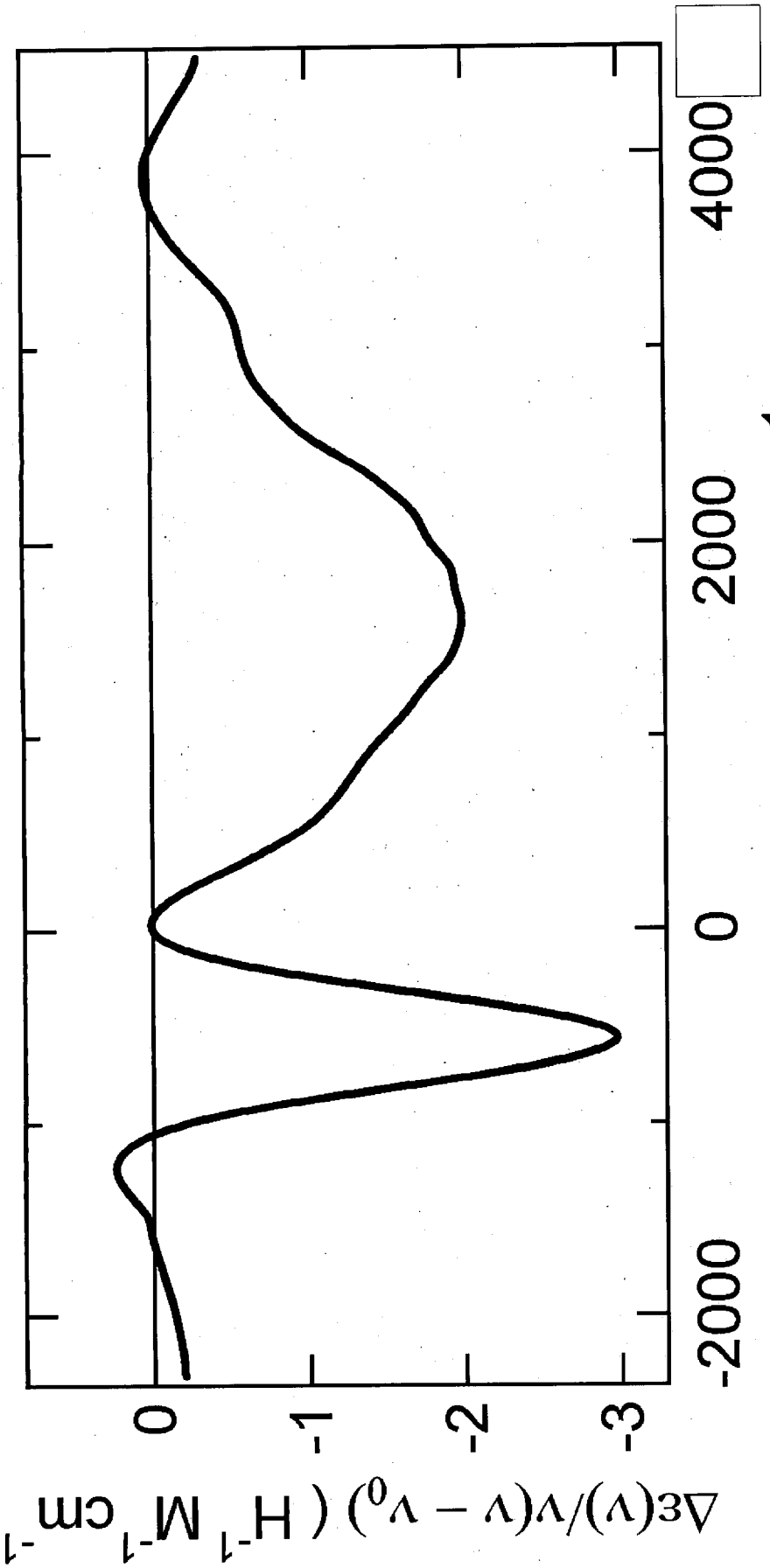

Figure 16. The integrand of the first moment of the MCD signal for the B band of deoxy Mb is plotted.

© 2002 American Chemical Society, J. Phys. Chem. B, Franzen jp025616k Supporting Info Page 29

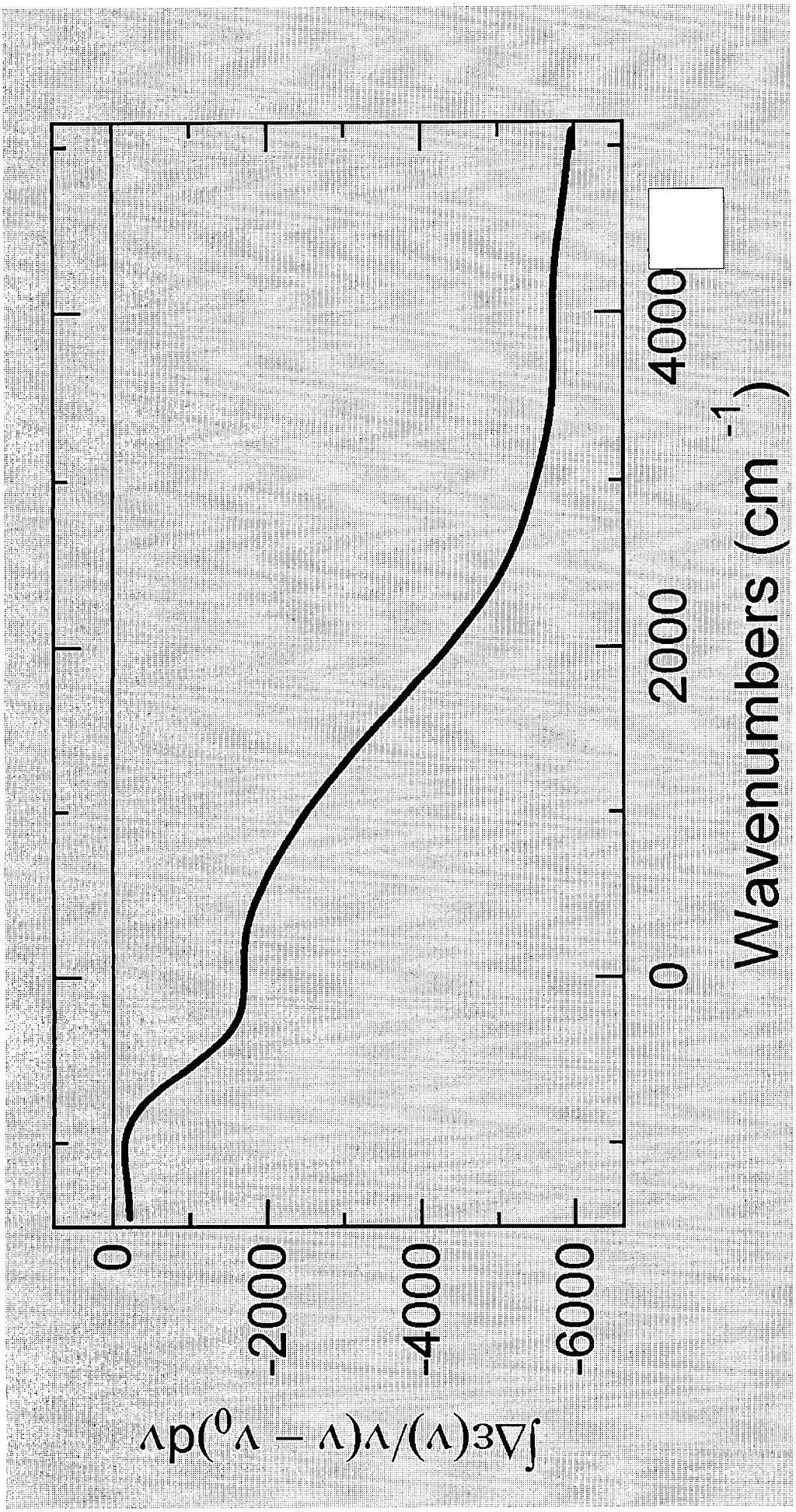

Figure 17. The integrated first moment of the MCD signal for the B band of deoxy Mb is plotted.

© 2002 American Chemical Society, J. Phys. Chem. B, Franzen jp025616k Supporting Info Page 30

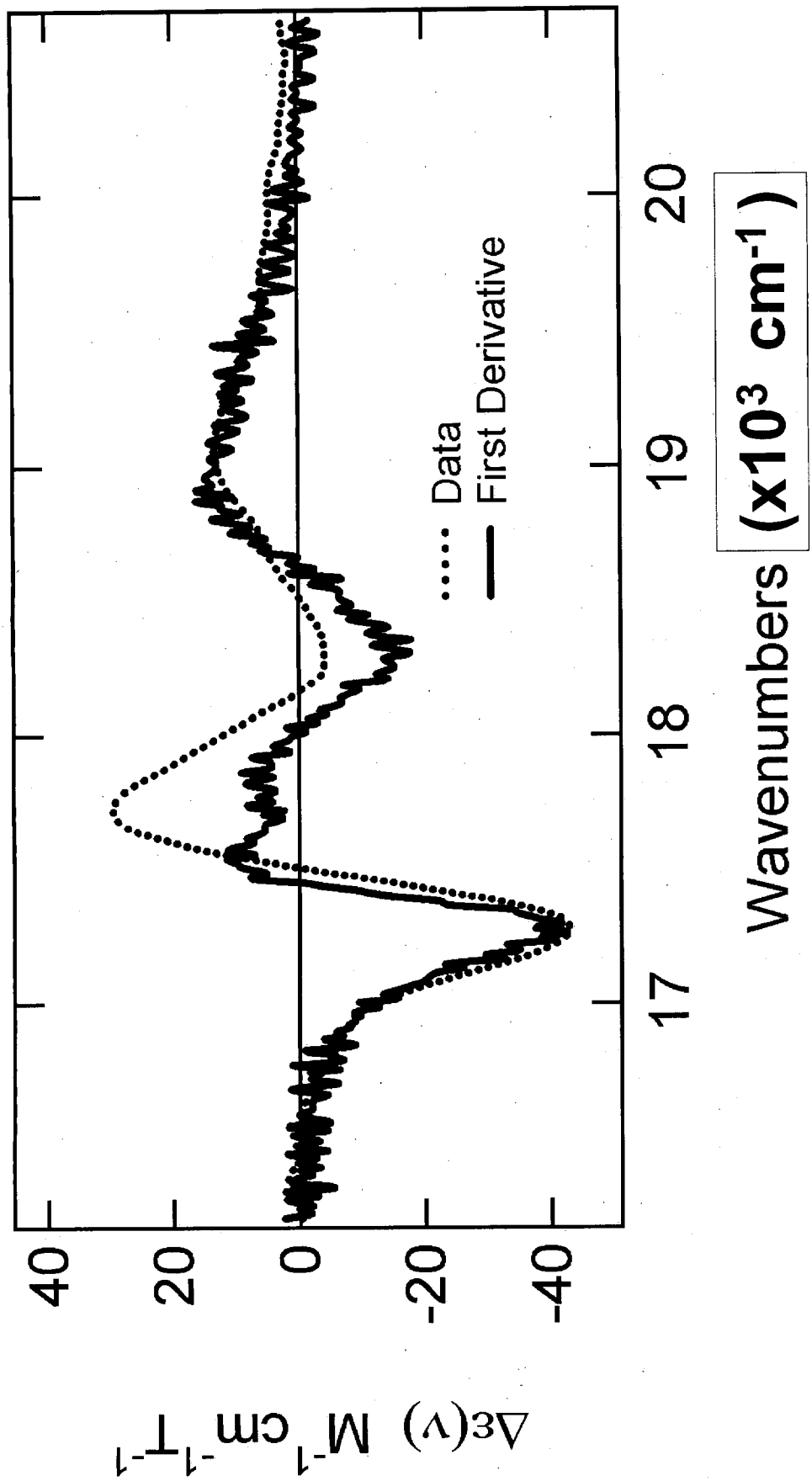

Figure 18. MCD spectrum of the Q band of MbCO. The MCD data are shown along with the calculated first derivative of the Q band absorption spectrum scaled by -1.2.

© 2002 American Chemical Society, J. Phys. Chem. B, Franzen jp025616k Supporting Info Page 31

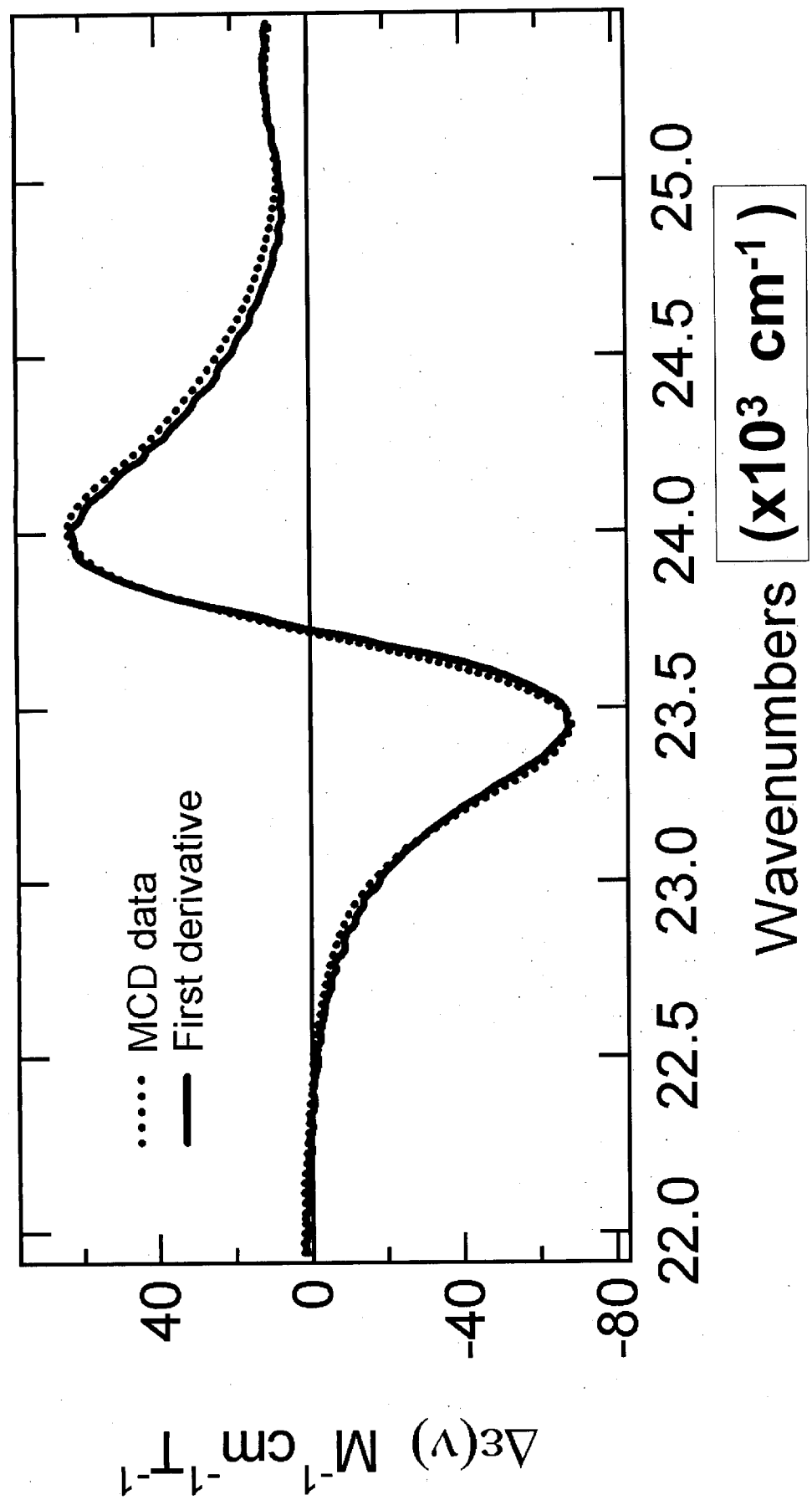

Figure 19. MCD spectrum of the B band of MbCO. The data are shown along with the calculated first derivative of the B band absorption spectrum scaled by -0.23.

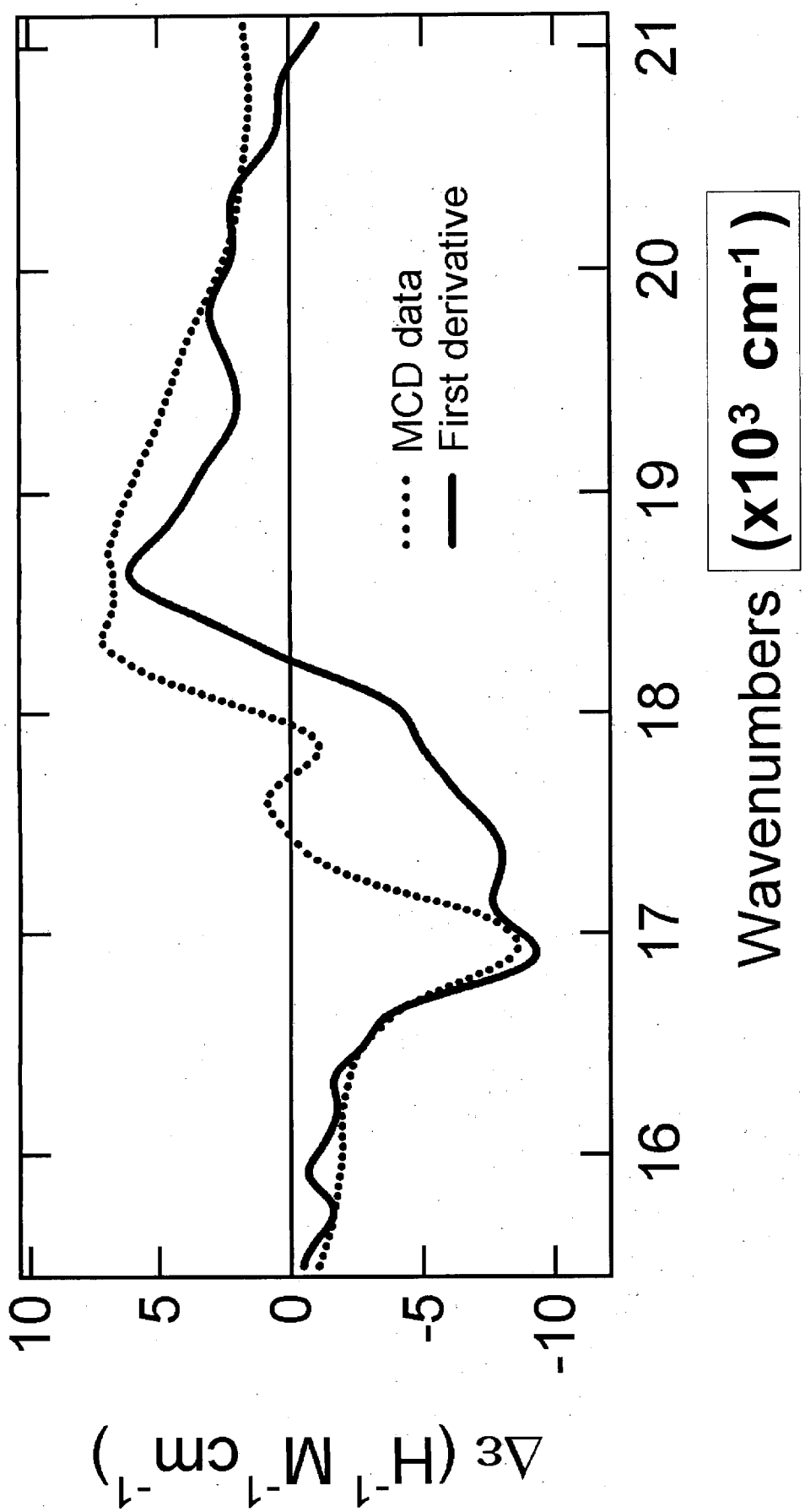

Figure 20. MCD spectrum of the Q band of deoxy Mb. The data are shown along with the calculated first derivative of the Q band absorption spectrum scaled by -1.0.

© 2002 American Chemical Society, J. Phys. Chem. B, Franzen jp025616k Supporting Info Page 33

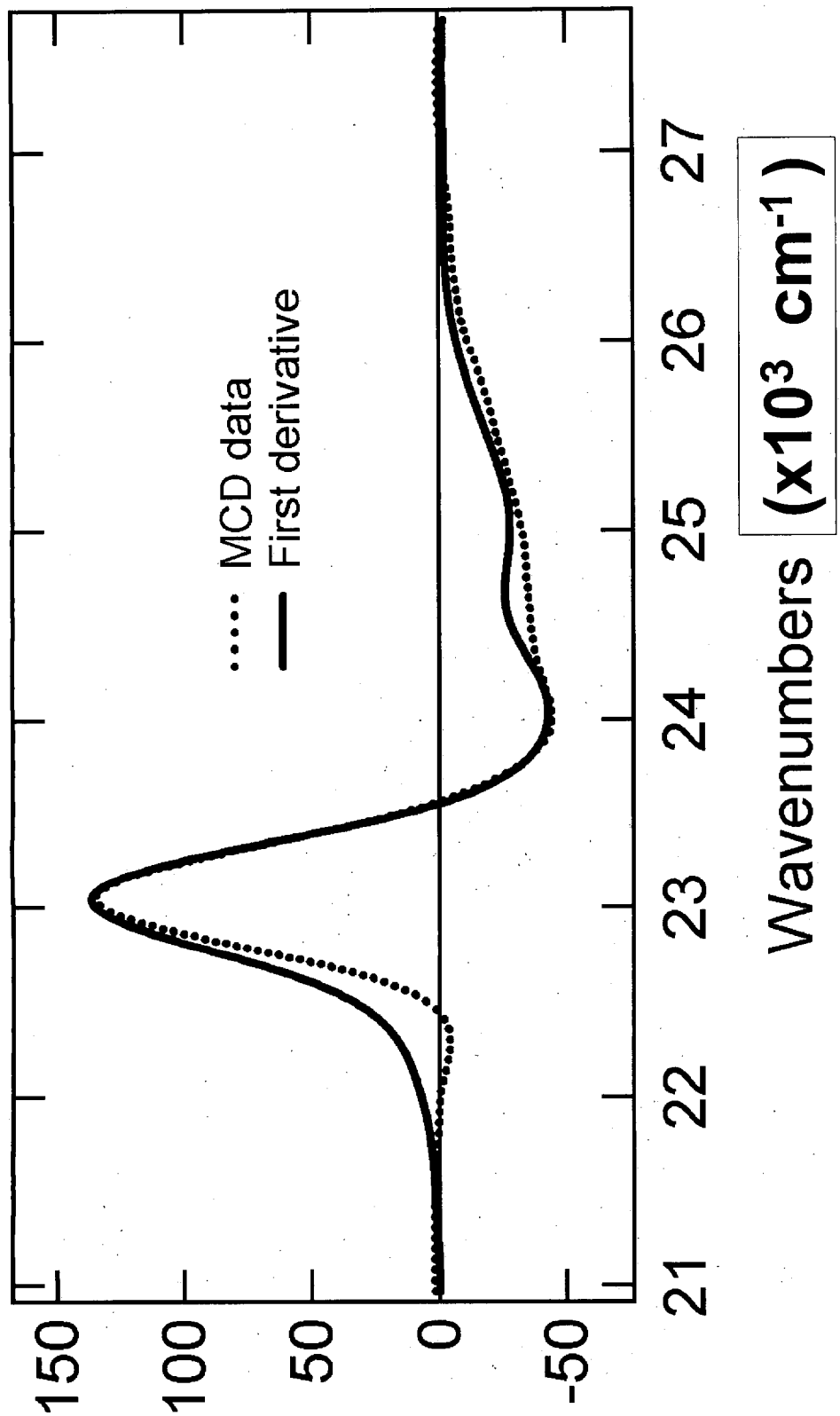

Figure 21. MCD spectrum of the B band of deoxy Mb. The data are shown along with the calculated first derivative of the B band absorption spectrum scaled by 0.9.